Waves and Instabilities in Dark Interstellar Molecular Clouds Containing Ferromagnetic Dust Grains[1]

A. A. Mamun[2] and P. K. Shukla

Institut für Theoretische Physik IV, Fakultät für Physik und Astronomie, Ruhr Universität Bochum,
D-44780 Bochum, Germany

Received January 15, 2002

The propagation characteristics of magnetization waves, as well as the instabilities of sound waves in a self-gravitating dark interstellar molecular cloud containing ferromagnetic dust grains and baryonic gas clouds, have been theoretically investigated by including the dynamics of both ferromagnetic dust grains and baryonic gases. It has been shown that there exist two types of subsonic or supersonic (depending on the field strength of the magnetization) transverse magnetization waves, which can be regarded as counterparts of Alfvén waves (for the parallel propagation) and magnetosonic waves (for the perpendicular propagation) in a magnetoactive plasma. It has also been found that, in addition to the usual Jeans instability, the sound waves suffer a new type of instability, which is due to the combined effects of the baryonic gas dynamics and self-gravitational field in both weakly and highly collisional regimes. © *2002 MAIK "Nauka/Interperiodica".*

PACS numbers: 98.38.Dq; 98.38.Am

Waves and instabilities in molecular clouds have become outstanding and challenging topics in space science and modern astrophysics because of their crucial role in understanding collapse, formation and evolution of interstellar molecular clouds, star formation, galactic structure and its evolution, etc. [1–10]. The instability of self-gravitating large gas clouds was first predicted by Jeans [1] about a hundred years ago. It was later rigorously investigated by a number of other distinguished physicists including Eddington [2], Chandrasekhar [3], Friedman and Polyachenko [4], Mestel and Spitzer [5], Spitzer [6], and others.

Theoretical studies [5–10] suggested that magnetic fields play a vital role in the evolution of interstellar clouds into self-gravitating star-forming regions. Mestel and Spitzer [5], as well as Spitzer [6], recognized the importance of ambipolar diffusion (a process by which the magnetic field carried by the ions diffuses through the neutral gas). Strittmatter [7] estimated the critical mass for gravitational collapse perpendicular to a magnetic field. Mouschovias [8, 9] rigorously investigated self-gravitating magnetic clouds by numerical simulations. Mouschovias and Spitzer [10] obtained an expression for the critical mass-to-magnetic flux ratio from the numerical studies of Mouschovias [8, 9].

On the other hand, Jones and Spitzer [11] provided a model for the existence of gas-dust interstellar mediums with a highly pronounced property of magnetic polarizability. This can be assumed due to a superparamagnetic dispersion of the fine ferromagnetic grains suspended in a gaseous cloud of molecular hydrogen. The regular galactic magnetic field threading such a medium introduces anisotropy in the orientation of permanently magnetized solid particles, tending to align their magnetic moments. The alignment of magnetic grains can be accompanied by filamentary agglomeration of dust particles (presumably by means of dipole–dipole interaction between magnetic moments of ferromagnetic grains) in the form of long-range magnetic chains extending along the direction of the regular magnetic field. Based on this model of Jones and Spitzer [11] and motivated by recent measurements of magnetic fields toward cores in magnetically supported dark interstellar clouds [12], Yang and Bastrukov [13] reported an alternative mechanism of large-scale wave motion in a one-component ferromagnetic neutral fluid. They suggested [13] that supersonic linewidths (inferred from the recent measurements of magnetic fields toward cores in magnetically supported dark interstellar clouds [12]) may be due to the transverse waves of magnetization propagating in such a one-component ferromagnetic neutral fluid.

The limitations of the analysis of [13] were that the ferromagnetic dust particles and baryonic gas molecules are assumed to be identical with a constant mass density [i.e., $m_d = m_b$ and $n_d = n_b = $ const are assumed, where m_d (m_b) is the mass of the ferromagnetic dust particle (baryonic gas molecule) and n_d (n_b) is the ferromagnetic dust particle (baryonic gas molecule) number density], and the effects of a self-gravitational field, collisions of dust particles with baryonic gas molecules, and the motions of ferromagnetic dust particles parallel to the direction of the magnetic moment were

---

[2] Permanent address: Department of Physics, Jahangirnagar University, Savar, Dhaka, Bangladesh.

neglected. However, in interstellar molecular clouds [14–20] $m_d \neq m_b$ and $n_d \neq n_b \neq$ const., and the effects of the self-gravitational field, collisions of dust particles with baryonic gas molecules, etc., cannot be neglected [14–20]. Thus, in order to study waves and instabilities in interstellar molecular clouds containing ferromagnetic dust particles [14–20], one must consider a two-component neutral fluid (ferromagnetic dust particles and baryonic gas molecules) and include the effects of mass density perturbations of the ferromagnetic dust fluid and the baryonic gas cloud, self-gravitational field, collisions of dust particles with baryonic gas molecules, etc. In this letter, we generalize the model of Yang Bastrukov [13] for a two-component (ferromagnetic massive dust fluid and baryonic gas cloud), self-gravitating, compressible fluid system including collisions. We have found that there exist two types of subsonic or supersonic (depending on the field strength of magnetization) transverse magnetization waves, and, in addition to the usual Jeans instability, the sound waves are subjected to a new type of instability which is due to the combined effects of the baryonic gas dynamics and self-gravitational field acting on massive dust particles.

We consider a model of a self-gravitating interstellar molecular cloud containing ferromagnetic dust particles and a baryonic gas cloud. These two fluids (ferromagnetic dust fluid and baryonic gas cloud) are assumed to be intercoupled via the gravitational interaction and dust-baryonic gas molecule collisions. For our purposes, we have the linearized basic equations describing the massive ferromagnetic dust fluid [13]

$$\partial \rho_d / \partial t + \rho_{d0} \nabla \cdot \mathbf{u_d} = 0, \tag{1}$$

$$\frac{\partial \mathbf{u_d}}{\partial t} = -\nabla \Psi + \frac{2 V_m^2}{m_0} \nabla \times (\mathbf{m} \times \hat{\mathbf{z}}) - \nu_{db}(\mathbf{u_d} - \mathbf{u_b}), \tag{2}$$

$$\frac{\partial \mathbf{m}}{\partial t} = \frac{m_0}{2}(\nabla \times \mathbf{u_d}) \times \hat{\mathbf{z}}; \tag{3}$$

the baryonic gas cloud [14],

$$\partial \rho_b / \partial t + \rho_{b0} \nabla \cdot \mathbf{u_b} = 0, \tag{4}$$

$$\frac{\partial \mathbf{u_b}}{\partial t} = -\nabla \Psi - \frac{C_b^2}{\rho_{b0}} \nabla \rho_b; \tag{5}$$

and the gravitational potential Ψ

$$\nabla^2 \Psi = 4\pi G(\rho_d + \rho_b), \tag{6}$$

where $\mathbf{u_d}$ ($\mathbf{u_b}$) is the dust fluid (baryonic gas cloud) velocity, ρ_d (ρ_{d0}) is the perturbed (equilibrium) dust fluid mass density, ρ_b (ρ_{b0}) is the perturbed (equilibrium) baryonic gas mass density, $\mathbf{m}_0 = \hat{\mathbf{z}} m_0$ is the perturbed (equilibrium) field of magnetization (magnetic moment per unit volume), $V_m = \sqrt{2\pi m_0^2/3\rho_{d0}}$ represents the speed of the magnetization wave [13], C_b represents the sound speed for the baryonic gas, ν_{db} is the collision frequency of ferromagnetic dust particles with baryonic gas molecules, and G is the universal gravitational constant.

To derive the dispersion relation for the perturbation waves, we assume that all perturbed quantities ρ_d, $\mathbf{u_d}$, $\mathbf{m}$, ρ_b, $\mathbf{u_b}$, and Ψ are proportional to $\exp(-i\omega t + \mathbf{k} \cdot \mathbf{r})$, where ω is the frequency and $\mathbf{k}$ is the wave propagation vector. Thus, substituting $\partial/\partial t = -i\omega$ and $\nabla = i\mathbf{k}$ into Eqs. (1)–(6), we have

$$(\Omega^2 - k_z^2 V_m^2)\mathbf{u_d} = -[V_\alpha^2(\mathbf{k} \cdot \mathbf{u_d}) + V_m^2 k_z u_z]\mathbf{k} + V_m^2[k^2 u_{dz} - k_z(\mathbf{k} \cdot \mathbf{u_d})]\hat{\mathbf{z}}, \tag{7}$$

where $\Omega^2 = \omega^2 + i\nu_{db}\omega$, $V_a^2 = \alpha_b \omega_{Jd}^2/k^2$, $\alpha_b = 1 - (\omega_{Jd}^2 - i\nu_{db}\omega)/(\omega^2 - k^2 C_b^2 + \omega_{Jd}^2)$, $\omega_{Jd} = \sqrt{4\pi G \rho_{d0}}$, and $\omega_{Jb} = \sqrt{4\pi G \rho_{b0}}$. From Eq. (7), we can express x, y, and z components of $\mathbf{u_d}$ as

$$(\Omega^2 - k_z^2 V_m^2 + k_x^2 V_\alpha^2)u_{dx} + k_x k_y V_\alpha^2 u_{dy} + k_x k_z (V_\alpha^2 + V_m^2)u_{dz} = 0, \tag{8}$$

$$k_y k_x V_\alpha^2 u_{dx} + (\Omega^2 - k_z^2 V_m^2 + k_y^2 V_\alpha^2)u_{dy} + k_y k_z (V_\alpha^2 + V_m^2)u_{dz} = 0, \tag{9}$$

$$k_z k_x (V_\alpha^2 + V_m^2)u_{dx} + k_z k_y (V_\alpha^2 + V_m^2)u_{dy} + [\Omega^2 - (k_x^2 + k_y^2)V_m^2 + k_z^2 V_\alpha^2]u_{dz} = 0. \tag{10}$$

Equations (8)–(10) then readily give a general dispersion relation,

$$\begin{vmatrix} \Omega^2 - k_z^2 V_m^2 + k_x^2 V_\alpha^2 & k_x k_y V_\alpha^2 & k_x k_z(V_\alpha^2 + V_m^2) \\ k_y k_x V_\alpha^2 & \Omega^2 - k_z^2 V_m^2 + k_y^2 V_\alpha^2 & k_y k_z(V_\alpha^2 + V_m^2) \\ k_z k_x(V_\alpha^2 + V_m^2) & k_z k_y(V_\alpha^2 + V_m^2) & \Omega^2 - (k_x^2 + k_y^2)V_m^2 + k_z^2 V_\alpha^2 \end{vmatrix} = 0. \tag{11}$$

We now assume that $\mathbf{k}$ lies in the y–z plane; i.e., $k_x = 0$. Thus, the dispersion relation (11) can be simplified as

$$(\Omega^2 - k_z^2 V_m^2)(\Omega^2 - k^2 V_m^2)(\Omega^2 + k^2 V_\alpha^2) = 0. \tag{12}$$

Equation (12) predicts three possible modes; namely, $\Omega^2 - k_z^2 V_m^2 = 0$, $\Omega^2 - k^2 V_m^2 = 0$, and $\Omega^2 + k^2 V_\alpha^2 = 0$. These three modes can be interpreted as follows.

A. The mode $\Omega^2 - k_z^2 V_m^2 = 0$: Substituting Ω, we can express this mode as

$$\omega^2 + i\nu_{db}\omega = k_z^2 V_m^2. \tag{13}$$

When $\nu_{db} \ll \omega$, we have a stable transverse mode of magnetization ($\omega^2 = k_z^2 V_m^2$) considered by Yang and Bastrukov [13]. On the other hand, when we consider $\nu_{db} \neq 0$ and assume $\omega = \omega_r + i\omega_i$, we have $\omega_r^2 = k_z^2 V_m^2 - \omega_i^2$ and $\omega_i = -\nu_{db}/2$. Accordingly, we have a damped mode with a damping rate $\nu_{db}/2$.

B. The mode $\Omega^2 - k^2 V_m^2 = 0$: Substituting Ω, we can express this mode as

$$\omega^2 + i\nu_{db}\omega = k^2 V_m^2. \tag{14}$$

The difference between mode (14) and mode (13) is that mode (14) contains the extra term $k_y^2 V_m^2$. Mode (14) represents a more general form of the dispersion relation for the obliquely propagating magnetization waves. We note that one cannot consider the perpendicular propagation of the magnetization waves from the dispersion relation (13) or from the dispersion relation for the magnetization waves derived by Yang and Bastrukov [13]. This is because of their taking curl of the ferromagnetic dust fluid velocity $\mathbf{u_d}$. We now compare the magnetization wave speed $V_m = \sqrt{2\pi m_0^2/3\rho_{d0}}$ with the Alfvén speed $V_A = \sqrt{B_0^2/4\pi\rho_{d0}}$ and with the isothermal sound speed $C_b = \sqrt{k_B T_b/m_b}$. Using $m_0 = 3B_0/8\pi$, we have $V_m/V_A \simeq 0.61$ and

$$\frac{V_m}{C_b} = \sqrt{\frac{3B_0^2 m_b}{32\pi n_{d0} m_d k_B T_b}}. \tag{15}$$

It is clear from $V_m/V_A \simeq 0.61$ that the magnetization-wave motions are sub-Alfvénic. Taking typical parameters for interstellar molecular clouds, i.e., considering one micron-sized ferromagnetic dust grains of the number density [15–18] $n_{d0} \simeq 10^{-7}$ cm^{-3}, the H_2 cloud [15–20] of the temperature $T_b \simeq 10$ K, and the number density $n_{b0} \simeq 10^3$ cm^{-3}, we have $V_m/C_b \simeq 0.4012$ for $B_0 \simeq 10$ μG and $V_m/C_b \simeq 1.003$ for $B_0 \simeq 25$ μG. This means that the magnetization-wave motions are subsonic for $B_0 < 25$ μG and supersonic for $B_0 \geq 25$ μG. However, Yang and Bastrukov [13] showed that the magnetization-wave motions are supersonic ($V_m/C_b \simeq 1.47$) for $B_0 \simeq 10$ μG. This discrepancy is due to the fact that Yang and Bastrukov [13] used $m_d = m_b = 3.9 \times 10^{-13}$ gm and $n_{d0} = n_{b0} = 10^3$ cm^{-3}, whereas we used $n_{d0} = 10^{-7}$ cm^{-3}, $n_{b0} = 10^3$ cm^{-3}, $m_d = 5 \times 10^{-13}$ gm (corresponding to one-micron-sized dust grains), and $m_b = 3.9 \times 10^{-24}$ gm. For these parameters ($n_{d0} = 10^{-7}$ cm^{-3}, $n_{b0} = 10^3$ cm^{-3}, $m_d = $

5×10^{-13} gm, and $m_b = 3.9 \times 10^{-24}$ gm), we also numerically estimated the Jeans frequency corresponding to the dust particles and the baryonic gas molecules. These are $\omega_{Jd} \simeq 2.05 \times 10^{-13}$ s^{-1} and $\omega_{Jb} \simeq 5.72 \times 10^{-14}$ s^{-1}, respectively.

C. The mode $\Omega^2 + k^2 V_\alpha^2 = 0$: Substituting Ω and V_α, we can express this mode as

$$(\omega^2 + i\nu_{db}\omega + \omega_{Jd}^2)(\omega^2 - k^2 C_b^2 + \omega_{Jb}^2)$$
$$= \omega_{Jd}^2(\omega_{Jb}^2 - i\nu_{db}\omega). \tag{16}$$

Equation (16) represents the sound waves associated with the baryonic gas molecules coupled by their collisions with dust particles and/or the self-gravitation field acting on dust particles and baryonic gas molecules. To explain it theoretically, we now consider two cases.

(i) Weakly collisional case: We consider the weakly collisional case, i.e., $\nu_{db} \ll \omega_{Jd}, \omega_{Jb}$, which allows one to express Eq. (16) as

$$\omega^4 + (\omega_J^2 - k^2 C_b^2)\omega^2 - \omega_{Jd}^2 k^2 C_b^2 = 0, \tag{17}$$

where $\omega_J = \sqrt{\omega_{Jb}^2 + \omega_{Jd}^2}$. When $\omega \gg kC_b$, we have from Eq. (17)

$$\omega^2 = k^2 C_b^2 - \omega_J^2. \tag{18}$$

This clearly represents a purely growing mode (since $\omega_J > kC_b$, in order to satisfy $\omega \gg kC_b$), where C_b plays the stabilizing role. This instability is just the usual Jeans instability and is well understood, since Jeans predicted the instability of self-gravitating large gas clouds [1].

On the other hand, when $\omega^2 \ll |\omega_J^2 - k^2 C_b^2|$, we have from Eq. (17)

$$\omega^2 = \frac{\omega_{Jd}^2 k^2 C_b^2}{(\omega_J^2 - k^2 C_b^2)}. \tag{19}$$

Equation (19) represents a new mode which is due to the combined effects of the baryonic gas dynamics and the self-gravitational field. This mode disappears if we neglect the baryonic-gas dynamics or the gravitational field acting on the dust grains. The important characteristics of this mode is that it is stable for $\omega_J > kC_b$, but is unstable (purely growing) for $\omega_J < kC_b$, which is opposite to the criterion for the Jeans instability.

(ii) Highly collisional case: We consider a very low-frequency mode in a highly collisional case, for which we can take $\nu_{db} \gg \omega$ and $|\omega_J^2 - k^2 C_b^2| \gg \omega^2$. These approximations allow one to express Eq. (16) as

$$\omega = i\frac{\omega_{Jd}^2 k^2 C_b^2}{\nu_{db}(k^2 C_b^2 - \omega_J^2)}. \tag{20}$$

This clearly indicates that this particular mode is purely damped for $\omega_J > kC_b$, but is purely growing (unstable) for $\omega_J < kC_b$. The instability is due to the combined effects of the baryonic gas dynamics and the self-gravitational field in a highly collisional regime.

To summarize, we have considered a two-component neutral fluid (one is a massive ferromagnetic dust fluid and another is a baryonic gas cloud) and investigated the properties of obliquely propagating sub-Alfvénic magnetization waves, as well as sound waves by including the effects of collisions, the self-gravitational field, and the dynamics of both ferromagnetic dust particles and baryonic gas molecules. We have shown that two types of transverse magnetization waves, which can be regarded as counterparts of Alfvén waves (for the parallel propagation; i.e., for $k_y = 0$) and of magnetosonic waves (for the perpendicular propagation; i.e., for $k_z = 0$) in a magnetoactive plasma. We have found that for typical interstellar molecular cloud parameters [15–20], e.g. $T_b \simeq 10$ K, $n_{b0} \simeq 10^3$ cm^{-3}, $m_b \simeq 3.9 \times 10^{-24}$ gm (mass of the hydrogen molecule), $n_{d0} \simeq 10^{-7}$ cm^{-3}, $m_d \simeq 5 \times 10^{-13}$ gm (corresponding to one-micron-sized dust grains), the magnetization-wave motions are supersonic for $B_0 \geq 25$ μG.

We have also investigated the sound waves propagating in a self-gravitating gas-dust medium containing tiny (micron sized) dust grains suspended in a cold gas cloud of molecular hydrogen. We have shown that in addition to the usual Jeans instability, the sound waves satisfying $\omega_J < kC_b < \omega_J$ and $\omega^2 \ll |k^2 C_b^2 - \omega_J^2|$ suffer a new type of instability which is due to the combined effects of the baryonic-gas dynamics and self-gravitational field in both weakly collisional [cf. Eq. (19)] and highly collisional [cf. Eq. (20)] limits.

REFERENCES

1. J. H. Jeans, Philos. Trans. R. Soc. London **199**, 1 (1902).

2. A. S. Eddington, *Internal Constitution of Stars* (Cambridge Univ. Press, Cambridge, 1926).

3. S. Chandrasekhar, *Hydrodynamic and Hydromagnetic Stability* (Clarendon, Oxford, 1961), Chap. XIII, p. 691.

4. A. M. Friedman and V. L. Polyachenko, *Physics of Gravitating Systems* (Nauka, Moscow, 1976; Springer-Verlag, Berlin, 1984).

5. L. Mestel and L. Spitzer, Mon. Not. R. Astron. Soc. **116**, 505 (1956).

6. L. Spitzer, Jr., *Physical Processes in Interstellar Medium* (Wiley, New York, 1978; Mir, Moscow, 1981).

7. P. A. Strittmatter, Mon. Not. R. Astron. Soc. **132**, 505 (1966).

8. T. Ch. Mouschovias, Astrophys. J. **206**, 753 (1976).

9. T. Ch. Mouschovias, Astrophys. J. **207**, 141 (1976).

10. T. Ch. Mouschovias and L. Spitzer, Astrophys. J. **210**, 326 (1976).

11. R. V. Jones and L. Spitzer, Astrophys. J. **146**, 943 (1967).

12. R. M. Crutcher, Astrophys. J. **520**, 706 (1999).

13. J. Yang and S. I. Bastrukov, Pis'ma Zh. Éksp. Teor. Fiz. **71**, 577 (2000) [JETP Lett. **71**, 395 (2000)].

14. D. Tsiklauri, New Astron. **5**, 361 (2000).

15. D. A. Mendis and M. Rosenberg, Annu. Rev. Astron. Astrophys. **32**, 419 (1994).

16. D. A. Mendis, in *Advances in Dusty Plasmas*, Ed. by P. K. Shukla, D. A. Mendis, and T. Desai (World Scientific, Singapore, 1997), p. 3.

17. P. K. Shukla and A. A. Mamun, *Introduction to Dusty Plasma Physics* (Institute of Physics Publ., Bristol, 2002).

18. G. E. Cliolek and T. Ch. Mouschovias, Astrophys. J. **418**, 774 (1993).

19. E. Zweibel, Phys. Plasmas **6**, 1725 (1999).

20. F. Nakamura, T. Matsumoto, T. Hanawa, and K. Tomisaka, Astrophys. J. **510**, 274 (1999).

Monopole Creation Operator in the Presence of Matter[1]

V. A. Belavin[1, *], M. N. Chernodub[1, 2, ***], and M. I. Polikarpov[1, **]

[1] *Institute of Theoretical Physics, Kanazawa University, 920-1192 Kanazawa, Japan*
* *e-mail: belavin@mccme.ru*
** *e-mail: polykarp@heron.itep.ru*
[2] *Institute of Theoretical and Experimental Physics, Moscow, 117259 Russia*
*** *e-mail: maxim@hep.s.kanazawa-u.ac.jp*
Received January 31, 2002

The monopole creation operator proposed recently by Fröhlich and Marchetti is investigated in the Abelian Higgs model with compact gauge field. We show numerically that the creation operator detects the condensation of monopoles in the presence of the dynamical matter field. © *2002 MAIK "Nauka/Interperiodica".*

PACS numbers: 12.38.Gc; 14.80.Hv

The value of deconfinement temperature is one of the most important predictions of the lattice QCD. To study the temperature phase transition, we have to investigate the order parameter. For full QCD, when dynamical quarks are taken into account, the string tension and the expectation value of the Polyakov line are not the order parameters. On the other hand, in the dual superconductor model of QCD vacuum [1], we have the natural order parameter for the confinement–deconfinement phase transition. This is the value of monopole condensate. It should be nonzero in the confinement phase (the monopoles are condensed as the Cooper pairs in ordinary superconductors) and zero in the deconfinement phase. To extract the monopole from vacuum of the non-Abelian fields, we have to perform the Abelian projection [2] and, after that, we can evaluate the value of monopole condensate using the monopole creation operator.

Originally, the gauge-invariant monopole-creation operator was proposed by Fröhlich and Marchetti for compact $U(1)$-gauge theory [3]. The construction is analogous to the Dirac creation operator [4] for a charged particle. The monopole operator was numerically studied in the compact Abelian gauge model [5] and in the pure $SU(2)$-gauge theory in the usual [6] and the spatial [7] Maximal Abelian gauges. It was found that the expectation value of this operator behaves as an order parameter for the confinement–deconfinement phase transition; the expected value is nonzero in the confinement phase and zero in the deconfinement phase. Similar conclusions were made for the other types of monopole-creation operators [8]. These results confirm the dual superconductor hypothesis [1] for a gluodynamics vacuum.

However, the monopole operator discussed in [3] exhibits some inconsistency in the presence of charged matter fields; namely, the Dirac string becomes visible. To get rid of the Dirac string dependence, a new monopole operator was proposed recently in [9]. Note that even the pure gluodynamics contains electrically charged fields in the Abelian projection: the off-diagonal gluons are (doubly) charged with respect to the diagonal gluon fields. Thus, the newly proposed operator [9] is more suitable for the investigation of confinement in SU(N)-gauge theories than the older operator [3]. The purpose of this paper is to check numerically whether the new monopole-creation operator is the order parameter in theories with matter fields. Below, we study the compact Abelian Higgs model in the London limit, keeping in mind further numerical investigation of the new monopole-creation operator in the non-Abelian gauge theories.

The original version of the gauge-invariant monopole-creation operator [3] in the compact $U(1)$-gauge theory is based on the duality of this model to the Abelian Higgs model. The Higgs field ϕ is associated with the monopole field, and the noncompact dual gauge field B_μ represents a dual photon. The gauge-invariant operator, which creates the monopole at the point x, can be written as the Dirac operator [4] in the dual model,

$$\Phi_x^{\mathrm{mon}}(H) = \phi_x e^{i(B, H_x)}, \qquad (1)$$

where the magnetic field of the monopole, **H**, is defined in the 3D time slice which includes the point x. By definition, the magnetic monopole field satisfies the Maxwell equation $\mathrm{div}\mathbf{H} = \delta^3(x)$, which guarantees the invariance of the operator Φ under the dual gauge transformation,

$$\phi \longrightarrow \phi e^{i\alpha}, \quad B \longrightarrow B + d\alpha. \qquad (2)$$

---

[1] This article was submitted by the authors in English.

The monopole-creation operator (1) can be rewritten in the original representation in terms of the compact field θ. In lattice notation, the expectation value of this operator is [3]

$$\langle \Phi^{\text{mon}} \rangle = \frac{1}{\mathscr{L}} \int_{-\pi}^{\pi} \mathscr{D}\theta \exp\{-S(d\theta + W)\},$$

$$\mathscr{L} = \int_{-\pi}^{\pi} \mathscr{D}\theta \exp\{-S(d\theta)\}.$$

(3)

For compact lattice electrodynamics, the general type of action satisfies the relation $S(d\theta + 2\pi n) = S(d\theta)$, $n \in \mathbb{Z}$. Besides the Coulomb monopole field H, the tensor form $W = 2\pi\delta\Delta^{-1}(H_x - \omega_x)$ depends on the Dirac string ω, which ends at the monopole position, $\delta^*\omega_x = {}^*\delta_x$, and is not restricted to the 3D time slice.

The operator (1) is well-defined for the theories without dynamical matter fields. However, if an electrically charged matter is added, then the creation operator (1) depends on the position of the Dirac string. To see this fact, we note that in the presence of the dynamical matter the dual gauge field B becomes compact. Indeed, as we mentioned above, the pure compact gauge model is dual to the noncompact $U(1)$ with matter fields [referred above to as the (dual) Abelian Higgs model]. Reading this relation backwards, we conclude that the presence of the matter field leads to the compactification of the dual gauge field B.

The compactness of the dual gauge field implies that the gauge transformation (2) must be modified:

$$\phi \longrightarrow \phi e^{i\alpha}, \quad B \longrightarrow B + d\alpha + 2\pi k,$$

(4)

where the compactness of the gauge field, $B \in (-\pi, \pi]$, is supported by the integer-valued vector field $k = k(B, \alpha)$. The role of the field k is to change the shape of the dual Dirac string attached to the magnetic charge in the dual theory. One can easily check that the operator (1) is not invariant under the compact gauge transformations (4):

$$\Phi_x^{\text{mon}}(H) \longrightarrow \Phi_x^{\text{mon}}(H)e^{2\pi i(k, H_x)}.$$

(5)

This fact was discussed in [9]. According to Eq. (5), if the field H is integer-valued, then operator (1) is invariant under the compact gauge transformations (4). This condition and the Maxwell equation require that field H has the form of a string attached to the monopole ("Mandelstam string"): $H_x \longrightarrow j_x, j \in \mathbb{Z}$. The string must be defined in the 3D time slice similarly to the magnetic field H. However, one can show that, for a fixed string position, the operator Φ creates a state with an infinite energy. This difficulty can be bypassed [9]

by the summation over all possible positions of the Mandelstam strings with some measure μ(j):

$$\Phi_x^{\text{mon, new}} = \phi_x \sum_{\substack{*j_x \in \mathbb{Z} \\ \delta^* j_x = \delta_x}} \mu(j_x)e^{i(B, j_m)}.$$

(6)

If Higgs field ϕ is q-charged ($q \in \mathbb{Z}$), the summation in Eq. (6) should be taken over q different strings, each of which carries the magnetic flux $1/q$. The transformation of $\Phi_x^{\text{mon, new}}$ to the original representation can easily be performed, and we get the expression similar to Eq. (3).

In this publication, we present the results of our numerical investigation of the operator $\Phi_x^{\text{mon, new}}$ (6) in the compact Abelian Higgs model with the action

$$S = -\beta\cos(d\theta) - \gamma\cos(d\varphi + q\theta),$$

(7)

where θ is the compact gauge field and φ is the phase of the Higgs field. For simplicity, we considered the London limit of the model, in which the radial part of the Higgs field is frozen. We calculated the (modified) effective constraint potential

$$V_{\text{eff}}(\Phi) = -\ln(\langle\delta(\Phi - \Phi^{\text{mon, new}})\rangle).$$

(8)

We simulated the 4D Abelian Higgs model on the 4^4, 6^4, and 8^4 lattice with $\gamma = 0.3$. The larger the charge q of the Higgs field, the easier the numerical calculation of $V_{\text{eff}}(\Phi)$. We performed our calculations for $q = 7$. For each configuration of 4D fields, we simulated a 3D model to get the Mandelstam strings with the weight $\mu(j_x)$, which we specify below. We generated 60 statistically independent 4D field configurations, and for each of these configurations we generated 40 configurations of 3D Mandelstam strings. We imposed the antiperiodic boundary conditions in space.

To define the measure μ in Eq. (6), we introduce the auxiliary 3D XY theory "living" on the time slice x^0 with the action

$$S(\chi, r) = \frac{\kappa}{2}\left\|\frac{d\chi - 2\pi B}{q} + 2\pi r\right\|^2,$$

(9)

where χ is 0-form with a value within $[-\pi q, \pi q]$ and r is **Z**-valued 1-form. One can prove that

$$\langle e^{i\chi_x}e^{-i\chi_R}\rangle_{R \to \infty}(B) \sim e^{i(B, H_x)}.$$

(10)

In space dimension $d \geq 3$, for sufficiently large κ and sufficiently small B, $\langle e^{i\chi_x}e^{-i\chi_y}\rangle \longrightarrow$ const as $|x - y| \longrightarrow \infty$. Moreover, the two-point function $\langle e^{i\chi_x}e^{-i\chi_R}\rangle(B)$ is periodic in B, with a period of 1. Hence, it has the Fourier representation similar to (6):

$$\langle e^{i\chi_x}e^{-i\chi_R}\rangle(B) = \frac{1}{\mathscr{L}} \sum_{\substack{j_x \in \frac{\mathbb{Z}}{q} \\ \delta j_x = \delta_x - \delta_R}} \mu(j_x)e^{i(B, j_m)},$$

(11)

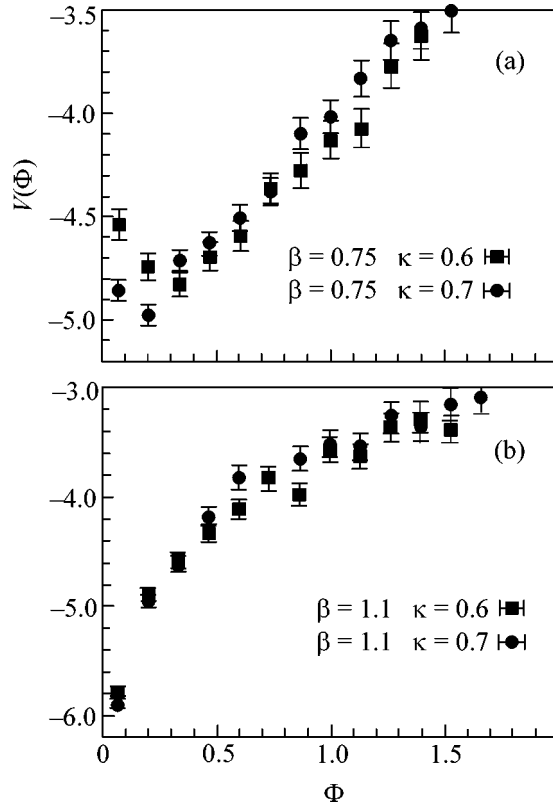**Fig. 1.** The effective monopole potential (8) in (a) confinement and (b) deconfinement phases.

Fig. 2. The effective monopole potential (8) in the low-κ region of the 3D model.

where the measure μ is defined by

$$\mu(j_x) = \exp\left\{-\frac{1}{2\kappa}\|j_x\|^2\right\}. \qquad (12)$$

Thus, in the theory with action (9) the two-point correlation function has the representation (10) analogous to the original representation (1) for the monopole-creation operator, and the dual representation (11) is analogous to the new representation (6) for the monopole-creation operator. Therefore, the measure in Eq. (6) should be defined by (12).

It is well known [10] that the 3D XY model in the Villain formulation has the phase transition for $\kappa_c(B = 0) \approx 0.32$. According to the suggestion of Fröhlich and Marchetti, the expectation value of the operator (6) should be the order parameter in the $\kappa > \kappa_c$ phase, where the density of the Mandelstam strings ρ is large enough. Our numerical observation has shown that, in the presence of the external field B, $\kappa_c(B) \approx 0.42$. In Fig. 1, we present the effective potential (8) in the confinement ($\beta = 0.85$) and the deconfinement ($\beta = 1.05$) phases for positive values of the monopole field. The potential is shown for two values of the 3D coupling constants $\kappa > \kappa_c$ corresponding to high densities of the Mandelstam strings. In the confinement phase (Fig. 1a),
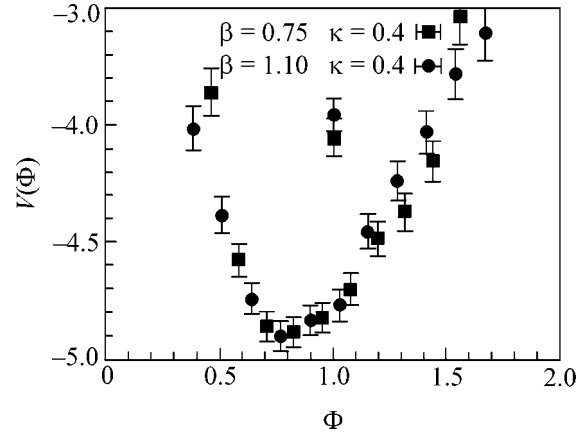
the potential $V(\Phi)$ has the Higgs form, signaling the monopole condensation. According to our numerical observations, this statement does not depend on the lattice volume. In the deconfinement phase (Fig. 1b), the potential has a minimum at $\Phi = 0$, which indicates the absence of the monopole condensate.

For small values of the 3D coupling constant κ (in the phase where Mandelstam strings j_x are not condensed), it was observed (Fig. 2) that the potential has the same behavior in both phases of the 4D model. Thus, the operator (6) serves as the order parameter for the deconfinement phase transition if the density of the Mandelstam strings is high; i.e., κ should be larger than $\kappa_c(B)$.

In summary, the new operator can be used as a test for the monopole condensation in the theories with electrically charged matter fields. Our calculations indicate that the operator should be defined in the phase where the Mandelstam strings are condensed, as was suggested by Fröhlich and Marchetti. The minimum of the potential corresponding to the value of the monopole condensate is zero in the deconfinement phase and nonzero in the confinement phase.

REFERENCES

1. G.'t Hooft, in *Proceedings of the EPS International Conference on High Energy Physics, Palermo, 1975*, Ed. by A. Zichichi (Compositori, Bologna, 1976); S. Mandelstam, Phys. Rep. **23**, 245 (1976).

2. G. 't Hooft, Nucl. Phys. B **190**, 455 (1981); M. N. Chernodub and M. I. Polikarpov, in *Confinement, Duality and Non-Perturbative Aspects of QCD*, Ed. by P. van Baal (Plenum, New York, 1998), p. 387; hep-th/9710205; A. Di Giacomo, Prog. Theor. Phys. Suppl. **131**, 161 (1998); R. W. Haymaker, Phys. Rep. **315**, 153 (1999).

3. J. Frohlich and P. A. Marchetti, Commun. Math. Phys. **112**, 343 (1987).

4. P. A. M. Dirac, Can. J. Phys. **33**, 650 (1955).

5. M. I. Polikarpov, L. Polley, and U. J. Wiese, Phys. Lett. B **253**, 212 (1991).

6. M. N. Chernodub, M. I. Polikarpov, and A. I. Veselov, Phys. Lett. B **399**, 267 (1997); Nucl. Phys. (Proc. Suppl.) **49**, 307 (1996).

7. M. N. Chernodub, M. I. Polikarpov, and A. I. Veselov, Pis'ma Zh. Éksp. Teor. Fiz. **69**, 166 (1999) [JETP Lett. **69**, 174 (1999)].

8. A. Di Giacomo and G. Paffuti, Phys. Rev. D **56**, 6816 (1997); Naoki Nakamura, Vitaly Bornyakov, Shinji Ejiri, *et al.*, Nucl. Phys. (Proc. Suppl.) **53**, 512 (1997).

9. J. Frohlich and P. Marchetti, Nucl. Phys. B **551**, 770 (1999); Phys. Rev. D **64**, 014505 (2001).

10. T. Banks, R. Myerson, and J. Kogut, Nucl. Phys. B **129**, 493 (1977).

Low-Energy Gluon to the Vacuum Polarization of Heavy Quarks[1]

S. Groote and A. A. Pivovarov*

Institut für Physik der Johannes-Gutenberg-Universität, Mainz, Germany
* Institute for Nuclear Research, Russian Academy of Sciences, Moscow, 117312 Russia
Received February 17, 2002

We calculate a correction to the effective electromagnetic current at low energies, induced by a heavy-quark loop, and determine the analytic structure of the vacuum polarization function at small q^2, for which an explicit expression is given to the $O(\alpha_s^3)$ order of perturbation theory. Implications to the high-precision analysis of experimental data on heavy-quark production in e^+e^- annihilation are discussed. © 2002 MAIK "Nauka/Interperiodica".

PACS numbers: 12.38.Bx; 12.20.Ds; 11.40.-q

High-precision tests of the standard model remain one of the main topics of particle phenomenology. Recent observation of a possible signal from the Higgs boson may complete the experimentally confirmed list of the standard model particles [1]. With improving precision of experimental data, more accurate theoretical formulas will be necessary for extracting numerical values of the standard model parameters. Recently, essential progress in high-order perturbation theory calculations for heavy quarks has been made, where a number of new physical effects have been described theoretically with high accuracy. The cross section of top–antitop production near the threshold was calculated at next-to-next-to-leading order of an expansion in the strong-coupling constant and the top quark velocity with an exact account of Coulomb interaction (for a review, see [2]). This allows the precise determination of the numerical value of the top quark mass at the next linear collider. The Coulomb resummation resides on a nonrelativistic approximation for the quark–antiquark system near the threshold, which was successfully used for the description of heavy-quark properties within the operator product expansion techniques and sum rules [3–5]. Being applied to the $b\bar{b}$ system, this method gives the best estimates of the b quark mass parameters [6–9].

In this work, we discuss the contribution of massless intermediate states to the correlators of heavy-quark currents. For the correlator of the vector currents, such a contribution first appears in the $O(\alpha_s^3)$ order of perturbation theory and is given by a three-gluon state. This gluon contribution to the correlator has a qualitatively new feature: its absorptive part starts at zero energy, in contrast to other contributions, where the absorptive parts start at the two-particle threshold. This feature determines the analytic structure of the correlator at small q^2; namely, in the $O(\alpha_s^3)$ order of perturbation theory, a cut along the positive semiaxis emerges. The nonanalyticity at the origin resulting from such a cut leads to strong limitations on the observables which can be theoretically constructed for confronting the experimental data. Because the data are most precise near the production threshold, the theoretical analysis should enhance this part of the spectrum. Technically, an enhancement of the near-threshold contributions is achieved by considering the integrals of production rate with weight functions which suppress the high-energy tail of the spectrum. The integrals with weight functions $1/s^n$ for the different positive integer n, $s = E^2$, where E is the total center-of-mass energy of the produced particles, are called moments of the spectral density and are most often used in the sum rule analysis. Theoretically, such moments are given by the derivatives at $q^2 = 0$ of the vacuum polarization function $\Pi(q^2)$, which is a basic quantity of the analysis of heavy-quark production in the $J^{PC} = 1^{--}$ channel. The vacuum polarization function is given by

$$i\int \langle T j_\mu(x) j_\nu(0) \rangle e^{iqx} d^4x = (q_\mu q_\nu - g_{\mu\nu} q^2)\Pi(q^2), \quad (1)$$

with the vector current $j^\mu = \bar{\psi}\gamma^\mu\psi$ of a heavy fermion ψ of the mass m. With the spectral density $\rho(s)$ defined by the relation

$$\rho(s) = \frac{1}{2\pi i}(\Pi(s+i0) - \Pi(s-i0)), \quad s > 0, \quad (2)$$

---

[1] This article was submitted by the authors in English.

the dispersion representation

$$\Pi(q^2) = \int \frac{\rho(s)ds}{s - q^2} \qquad (3)$$

holds. The integral in Eq. (3) runs over the whole spectrum of the correlator in Eq. (1) or over the whole support of the spectral density $\rho(s)$ in Eq. (2). A necessary ultraviolet regularization (subtractions, for instance) is assumed in Eq. (3). The moments of spectral density $\rho(s)$ of the form

$$\mathcal{M}_n = \int \frac{\rho(s)ds}{s^{n+1}} \qquad (4)$$

are usually studied within the sum-rule method for heavy quarks [10]. These moments are related to the derivatives of the vacuum polarization function $\Pi(q^2)$ at the origin as

$$\mathcal{M}_n = \frac{1}{n!}\left(\frac{d}{dq^2}\right)^n \Pi(q^2)\Big|_{q^2=0}. \qquad (5)$$

Such moments are chosen in order to suppress the high-energy part of the spectral density $\rho(s)$, which is not measured accurately in experiments. Within the sum-rule method, one believes that the theoretical expressions for the moments in Eq. (4) or, equivalently, the derivatives in Eq. (5) exist, i.e., formally lead to the well-defined quantities for any n. The existence of moments seems to be obvious because of the implicit assumption that the spectral density $\rho(s)$ of the correlator of the heavy-quark electromagnetic currents vanishes below the two-particle threshold $s = 4m^2$, which means that the vacuum polarization function of heavy quarks $\Pi(q^2)$ is analytic over the whole complex plane of q^2, except for the cut along the positive real axis starting at $4m^2$. This assumption about the analytic properties of the vacuum polarization function $\Pi(q^2)$ is valid to the first few orders of perturbation theory. However, its validity in a full theory depends of the details of interaction. For instance, the resummation of Coulomb effects to all orders may result in the appearance of bound states below the perturbation theory threshold $s = 4m^2$. Still, this is only true for the attractive Coulomb interaction, while the repulsive Coulomb interaction modifies the shape of the free-particle spectrum but does not change its support, i.e., does not lead to bound-state formation below the continuum spectrum. The assumption that the moments in Eq. (4) exist for any n may also be incorrect in high orders of perturbation theory in models with massless particles, for example, in QCD with massless gluons. In QCD, in the $O(\alpha_s^3)$ order of perturbation theory, there is a contribution of massless states to the correlator in Eq. (1), which leads to the infrared (small s) divergence of theoretical expressions for the moments for large n because of the branching-point (cut) singularity of $\Pi(q^2)$ at the origin.

We determine the behavior of the vacuum-polarization function $\Pi(q^2)$ at small q^2 ($q^2 \ll m^2$) as

$$\Pi(q^2)\Big|_{q^2 \approx 0} = \frac{C_g}{12\pi^2}\left(\frac{q^2}{4m^2}\right)^4 \ln\left(\frac{\mu^2}{-q^2}\right), \qquad (6)$$

with

$$C_g = \frac{17}{243\,000}d_{abc}d_{abc}\left(\frac{\alpha_s}{\pi}\right)^3. \qquad (7)$$

Here, d_{abc} are the totally symmetric structure constants of the $SU(N_c)$-gauge group defined by the relation $d_{abc} = 2\mathrm{tr}(\{t^a, t^b\}t^c)$, and t^a are generators of the group with normalization $\mathrm{tr}(t^a, t^b) = 1/2$. For the $SU(3)$-gauge group of QCD, one has $d_{abc}d_{abc} = 40/3$. The parameter μ in Eq. (6) is the renormalization point.

The singularity of the vacuum-polarization function given in Eq. (6) (a cut along the positive real axis in the complex q^2 plane) prevents one from calculating moments of the spectral density in Eq. (4) with $n \geq 4$. Indeed, the high-order derivatives of $\Pi(q^2)$ at the origin determining the high-order moments, according to Eq. (5), do not exist for $n \geq 4$ because of a branching-point singularity, as one can see from Eq. (6). In terms of moments, one can see this by calculating the behavior of the spectral density at small squared energies s,

$$\rho(s)\Big|_{s \approx 0} = \frac{C_g}{12\pi^2}\left(\frac{s}{4m^2}\right)^4, \qquad (8)$$

which makes the integrals in Eq. (4) divergent at small s for $n \geq 4$. The formulas for the vacuum-polarization function in Eqs. (6) and (7) are given for a heavy quark in the $SU(N_c) \otimes U(1)$-gauge model. The result for QED may be obtained by substituting $\alpha_s \longrightarrow \alpha$ for the coupling constant and by changing the group factors; the contribution is, however, very small and of no practical interest. Contributions of light (massless) quarks appear in the $O(\alpha_s^4)$ order of perturbation theory and are neglected.

We present the derivation of our result given by Eqs. (6) and (7) and briefly discuss some consequences for the phenomenology of heavy quarks. Note that the induced current is a correction on the order of $1/m^4$ in the inverse heavy-quark mass, which vanishes in the limit of an infinitely heavy quark. Corrections in inverse heavy-quark masses are important for tests of the standard model at the present level of precision and have already been discussed in various areas of particle phenomenology [11–13].

A correction to the electromagnetic current due to a virtual heavy-quark loop is given by the transition of a photon to three gluons (see figure). Two-gluon transitions are forbidden, according to the generalization of Farry's theorem to the nonabelian theories [14]. We are interested in the behavior of the transition amplitude at low energies and take the limit of a very heavy quark.

Formally, the limit $m \longrightarrow \infty$ is taken, which, in physical terms, means that m is much larger than all momenta of the external legs of the diagram, namely, three gluons and a photon. The induced current J^μ is written in a covariant form as a derivative of the antisymmetric operator $\mathbb{O}_{\mu\nu}$ built only from the gluon fields,

$$J^\mu = \partial_\nu \mathbb{O}^{\mu\nu}, \quad \mathbb{O}^{\mu\nu} + \mathbb{O}^{\nu\mu} = 0. \qquad (9)$$

This structure of the induced current automatically guarantees the current conservation

$$\partial_\mu J^\mu = 0, \qquad (10)$$

as it should be for the electromagnetic current. The straightforward calculation gives the result for the induced correction

$$J^\mu = \frac{-g_s^3}{1440\pi^2 m^4}(5\partial_\nu \mathbb{O}_1^{\mu\nu} + 14\partial_\nu \mathbb{O}_2^{\mu\nu}), \qquad (11)$$

with

$$\mathbb{O}_{1\mu\nu} = d_{abc}G_{\mu\nu}^a G_{\alpha\beta}^b G_{\alpha\beta}^c, \quad \mathbb{O}_{2\mu\nu} = d_{abc}G_{\mu\alpha}^a G_{\alpha\beta}^b G_{\beta\nu}^c, \qquad (12)$$

where $G_{\mu\nu}^a$ is a gauge-field strength tensor for the gauge group $SU(N_c)$.

A correlator of the induced current J^μ has the general form

$$\langle TJ^\mu(x)J^\nu(0)\rangle = -\partial_\alpha\partial_\beta\langle T\mathbb{O}^{\mu\alpha}(x)\mathbb{O}^{\nu\beta}(0)\rangle, \qquad (13)$$

where the explicit expression of the current as a derivative of the antisymmetric operator $\mathbb{O}^{\mu\nu}$ is used. The resulting correlator $\langle T\mathbb{O}^{\alpha\beta}(x)\mathbb{O}^{\nu\beta}(0)\rangle$ in Eq. (13) contains only gluonic operators. To the leading order, the correlator in Eq. (13) has the topological structure of a sunset diagram, which is readily computed in the configuration space [15]. We find

$$\langle TJ_\mu(x)J_\nu(0)\rangle$$
$$= -\frac{34}{2025\pi^4 m^8}\left(\frac{\alpha_s}{\pi}\right)^3 d_{abc}d_{abc}(\partial_\mu\partial_\nu - g_{\mu\nu}\partial^2)\frac{1}{x^{12}}. \qquad (14)$$

The Fourier transform of the correlator in Eq. (14) reads

$$i\int\langle TJ_\mu(x)J_\nu(0)\rangle e^{iqx}d^4x$$
$$= (q_\mu q_\nu - q_{\mu\nu}q^2)\frac{C_g}{12\pi^2}\left(\frac{q^2}{4m^2}\right)^4\ln\left(\frac{\mu^2}{-q^2}\right), \qquad (15)$$

with the constant C_g taken from Eq. (7). The spectral density of the polarization function in Eq. (15) is given in Eq. (8).

The spectral density of the correlator in Eq. (14) can be found without explicit calculation of its Fourier transform. Instead, one can use the spectral decomposi-
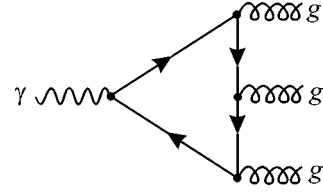
Heavy-quark loop correction to the electromagnetic current.

tion (dispersion representation) in the configuration space,

$$\frac{i}{x^{12}} = \frac{\pi^2}{2^8\Gamma(6)\Gamma(5)}\int_0^\infty s^4 D(x^2, s)ds, \qquad (16)$$

with $D(x^2, s)$ being the propagator of a scalar particle of mass $\sqrt{s}$, and

$$D(x^2, m^2) = \frac{im\sqrt{-x^2}K_1(m\sqrt{-x^2})}{4\pi^2(-x^2)}, \qquad (17)$$

where $K_1(z)$ is a McDonald function (a modified Bessel function of the third kind; see, e.g., [16]). $\Gamma(z)$ is the Euler's gamma function.

Note that the three-gluon contribution to the spectral density of the quark-current correlator in Eq. (1) for large energies (when the limit of massless quarks can be used) is well known and reads [17–19]

$$\left(\frac{\alpha_s}{\pi}\right)^3\frac{d_{abc}d_{abc}}{1024}\left(\frac{176}{3} - 128\zeta(3)\right). \qquad (18)$$

Here, $\zeta(z)$ is Riemann's ζ function.

One immediate application of our result consists in the precise determination of heavy-quark parameters from the data on heavy-quark production. Because of the low-energy gluon contributions, the large n ($n \geq 4$) moments of the spectral density do not formally exist. The range of n used in original considerations of sum rules and in some recent analyses requires the proper modification of theoretical expressions for the moments in order to account for this new contribution at the $O(\alpha_s^3)$ level of precision. For the $c\bar{c}$ system, the moments with $n \sim 3$–7 [10, 20] were analyzed. For the precision analysis of $b\bar{b}$ production, the sum rules for the moments with larger $n \sim 5$–20 were studied in the literature. In view of our results, the modification of the analysis is necessary at the formal level of the $O(\alpha_s^3)$ accuracy of perturbation theory. Note that the considered correction is of the same order in α_s as the contribution of Coulomb bound states, which is known to be numerically important for the description of Υ reso-

nances. The restriction of using only the first few moments with $n < 4$ seems to be unsatisfactory from the phenomenological point of view. For small n, the high-energy contribution, which is not known experimentally with reasonable precision, is not sufficiently suppressed and introduces a large quantitative uncertainty in the sum rules for the moments.

A modified analysis can be based on the theoretical expression for the derivatives of the correlator at some infrared safe point $q^2 = -\Delta < 0$ [21]. For the infrared regularized moments

$$\mathcal{M}_n(\Delta) = \frac{1}{n!}\left(\frac{d}{dq^3}\right)^n \Pi(q^2)\Bigg|_{q^2 = -\Delta} = \int_0^\infty \frac{\rho(s)ds}{(s+\Delta)^{n+1}}, \quad (19)$$

there is no divergence at small s. The infrared regularization parameter Δ should be small, because the continuum contribution to the moments is not suppressed for large values of Δ even for sufficiently large n. However, it cannot be arbitrarily small because the resulting correlator of gluonic currents at low energies in Eq. (13) is essentially normalized at $\mu^2 = \Delta$ if radiative corrections are taken into account. Therefore, Δ should be large enough for the perturbation theory calculations to be justified [22, 23]. On the experimental side of the sum rules, it is rather difficult to evaluate the part of the spectral integral over the low-energy gluons because of mixing with light-quark contributions. These theoretical and experimental constraints on the numerical value of the parameter Δ require special analysis of the accuracy attainable with the infrared-regularized sum rules in Eq. (19).

Another possibility to bypass the problem of infrared divergence is to use finite-energy sum rules without $1/s^n$ weight functions that are free from the infrared problem [24] or to apply a direct subtraction of the three-gluon contribution, as was been proposed in [25].

To conclude, we have presented a correction to the electromagnetic current induced by a virtual heavy-quark loop that is relevant to an effective theory of light degrees of freedom at low energies. The spectrum of the correlator of such an induced current starts at zero energy. This fact necessitates the modification of the standard analysis of the moment sum rules for the $b\bar{b}$ system to the $O(\alpha_s^3)$ order of perturbation theory.

REFERENCES

1. R. Barate *et al.* (ALEPH Collab.), Phys. Lett. B **495**, 1 (2000); M. Acciarri *et al.* (L3 Collab.), Phys. Lett. B **495**, 18 (2000).
2. A. H. Hoang, M. Beneke, K. Melnikov, *et al.*, Eur. Phys. J. C **3**, 1 (2000).
3. M. B. Voloshin, Nucl. Phys. B **154**, 365 (1979).
4. H. Leutwyler, Phys. Lett. B **98**, 447 (1981).
5. M. B. Voloshin, Int. J. Mod. Phys. A **10**, 2865 (1995); M. B. Voloshin and Y. M. Zaitsev, Usp. Fiz. Nauk **152**, 361 (1987) [Sov. Phys. Usp. **30**, 553 (1987)].
6. J. H. Kühn, A. A. Penin, and A. A. Pivovarov, Nucl. Phys. B **534**, 356 (1998); A. A. Penin and A. A. Pivovarov, Phys. Lett. B **435**, 413 (1998); Nucl. Phys. B **549**, 217 (1999).
7. K. Melnikov and A. Yelkhovsky, Phys. Rev. D **59**, 114009 (1999).
8. A. H. Hoang, Phys. Rev. D **61**, 034005 (2000).
9. Y. Kiyo and Y. Sumino, Phys. Lett. B **496**, 83 (2000).
10. V. A. Novikov, L. B. Okun, M. A. Shifman, *et al.*, Phys. Rep. C **41**, 1 (1978).
11. A. A. Pivovarov, Pis'ma Zh. Éksp. Teor. Fiz. **53**, 510 (1991) [JETP Lett. **53**, 536 (1991)]; Phys. Lett. B **263**, 282 (1991); A. A. Penin and A. A. Pivovarov, Phys. Rev. D **49**, 265 (1994); Fiz. Élem. Chastits At. Yadra **29**, 702 (1998) [Phys. Part. Nucl. **29**, 286 (1998)].
12. K. G. Chetyrkin, Phys. Lett. B **307**, 169 (1993).
13. S. A. Larin, T. van Ritbergen, and J. A. Vermaseren, Nucl. Phys. B **438**, 278 (1995).
14. N. V. Smolyakov, Theor. Math. Phys. **50**, 225 (1982).
15. S. Groote, J. G. Körner, and A. A. Pivovarov, Phys. Lett. B **443**, 269 (1998); Nucl. Phys. B **542**, 515 (1999); Eur. Phys. J. C **11**, 279 (1999); S. Narison and A. A. Pivovarov, Phys. Lett. B **327**, 341 (1994).
16. G. N. Watson, *Theory of Bessel Functions* (Cambridge Univ. Press, Cambridge, 1944).
17. S. G. Gorishnii, A. L. Kataev, and S. A. Larin, Phys. Lett. B **259**, 144 (1991).
18. K. G. Chetyrkin, Phys. Lett. B **391**, 402 (1997).
19. L. R. Surguladze and M. A. Samuel, Phys. Rev. Lett. **66**, 560 (1991); **66**, 2416 (1991).
20. S. N. Nikolaev and A. V. Radyushkin, Phys. Lett. B **124**, 243 (1983).
21. L. J. Reinders, H. Rubinstein, and S. Yazaki, Phys. Rep. **127**, 1 (1985).
22. A. L. Kataev, N. V. Krasnikov, and A. A. Pivovarov, Phys. Lett. B **107**, 115 (1981); Nucl. Phys. B **198**, 508 (1982); **490**, 505 (1997); A. A. Pivovarov, Yad. Fiz. **63**, 1734 (2000) [Phys. At. Nucl. **63**, 1646 (2000)].
23. T. Inami, T. Kubota, and Y. Okada, Z. Phys. C **18**, 69 (1983).
24. N. V. Krasnikov and A. A. Pivovarov, Phys. Lett. B **112**, 397 (1982); N. V. Krasnikov, A. A. Pivovarov, and A. N. Tavkhelidze, Z. Phys. C **19**, 301 (1983).
25. J. Portoles and P. D. Ruiz-Femenia, Report No. IFIC/01-39; hep-ph/0107324.

Two-Photon Spectron

M. V. Chekhova

Moscow State University, Vorob'evy gory, Moscow, 119899 Russia

e-mail: masha@qopt.ilc.msu.su

Received February 7, 2002

The propagation of a two-photon light in a transparent medium with group velocity dispersion is considered. It is shown that, even in the stationary case of two-photon light generation by cw pumping, the second-order light correlation function behaves like a short pulse: when propagating in a medium, this function smears and at large distances acquires the spectral shape of two-photon radiation. © *2002 MAIK "Nauka/Interperiodica".*

PACS numbers: 42.50.Dv; 42.81.Dp

Two-photon light is ordinarily obtained in experiments with spontaneous parametric scattering (SPS) [1]; it is of considerable interest in the context of generating so-called entangled states in optics. At present, the use of two-photon light for quantum information transmission is the subject of animated discussion [2].

In the simplest form, the state vector of radiation generated in SPS can be written, with allowance for the polarization, as $|\Psi_I\rangle = |vac\rangle + c|2, 0\rangle$ for the type-I matching and $|\Psi_{II}\rangle = |vac\rangle + c|1, 1\rangle$ for the type-II matching. In these expressions, $|n, m\rangle$ denotes the state with n photons in the polarization mode x and m photons in the polarization mode y; the parameter $c \ll 1$ specifies the amplitude of a two-photon state, and $|vac\rangle$ stands for the vacuum state. However, this expression is rather idealistic: in reality, the spectrum, both frequency and angular, of a two-photon light is always of a finite length. For example, in the case of frequency-degenerate matching, the state generated in the SPS from cw pumping has the form of spectral decomposition [3]:

$$|\Psi\rangle = |vac\rangle + c\int d\Omega F(\Omega) a_s^\dagger\left(\frac{\omega_p}{2} - \Omega\right) a_i^\dagger\left(\frac{\omega_p}{2} + \Omega\right)|vac\rangle$$

$$\equiv |vac\rangle + c\int d\Omega F(\Omega)\left|\frac{\omega_p}{2} - \Omega\right\rangle_s\left|\frac{\omega_p}{2} + \Omega\right\rangle_i, \tag{1}$$

where ω_p is the pump frequency, and the indices i and s correspond to the idler and signal modes, respectively. These may be the polarization (for the type-II matching) or spatial modes. The amplitude $F(\Omega)$, usually called the biphoton amplitude,[1] determines the spectral

---

[1] A biphoton is referred to as a pair of photons with correlated moments of creation, frequencies, wave vectors, and polarizations.

properties of a two-photon light. It has different forms for the type-II and type-I matchings:

$$F_{II}(\Omega) = \frac{\sin(DL\Omega/2)}{DL\Omega/2},$$

$$F_I(\Omega) = \frac{\sin(D''L\Omega^2/2)}{D''L\Omega^2/2}, \tag{2}$$

where L is the length of nonlinear crystal, D is the difference in the reciprocal group velocities of the signal and idler photons in the nonlinear crystal, and D'' is the second derivative of the dispersion relation $k(\omega)$ in the nonlinear crystal. One can see from Eq. (1) that, in the presence of spectral distribution, the light emitted in SPS always occurs in the entangled state.

The spectrum of a two-photon light in the vicinity of the degenerate phase-matching frequency $\omega_p/2$ is determined by the square of the modulus of the spectral amplitude $F(\Omega)$. Accordingly, the first-order correlation function has the form

$$G^{(1)}(\tau) = 4|c|^2\exp\left\{-i\frac{\omega_p}{2}\tau\right\}\int d\Omega|F(\Omega)|^2\cos(\Omega\tau). \tag{3}$$

For the second-order correlation function, calculations give the following expression:

$$G^{(2)}(\tau) = 4|c|^2\left|\int d\Omega F(\Omega)\cos(\Omega\tau)\right|^2. \tag{4}$$

For SPS in crystals with a length on the order of 1 cm, the typical width of the second-order correlation function is equal to several tens or hundreds of femtoseconds.

Let us now consider the propagation of two-photon light in a transparent dispersion medium. In the vicinity of degenerate matching, the dispersion relation in this medium can be written as $k(\omega) = k(\omega_p/2) + k'(\omega_p/2)(\omega - \omega_p/2) + k''(\omega_p/2)(\omega - \omega_p/2)^2/2$. It is well known that the

third term in this expansion is responsible for the smearing of short pulses in the medium. For the extended dispersion medium, $z \gg l_d$, where the dispersion length can be defined as $l_d = \tau_0^2/2pk''$ and τ_0 is the initial pulse duration, the pulse acquires a shape coinciding with its spectrum. Such a pulse has come to be known in the literature as a "spectron" [4].

Quite the same effect arises for two-photon light propagating in a dispersion medium. In this case, the creation operators $a_{s,i}^+(\omega_p/2 \pm \Omega)$ in Eq. (1) assume frequency-dependent phase factors, which can be interpreted as the appearance of a factor $\exp\{i(k_i'' + k_s'')\Omega^2 z/2\}$ for the spectral amplitude $F(\Omega)$. As a result, the first-order correlation function, as well as the spectrum, does not change. However, the second-order correlation function (4), which contains $F(\Omega)$ instead of $|F(\Omega)|^2$ under the integral sign, changes. Since the relation between $F(\Omega)$ and $G^{(2)}(\tau)$ is analogous to the relation between the pulse spectral amplitude and the square of the pulse envelope, the second-order correlation function behaves like a short pulse propagating in a dispersion medium. For $z \gg l_d$ (as in the femtosecond pulse optics, this condition may be called "far zone" condition), the correlation function has the form

$$G^{(2)}(\tau) \sim |F(\Omega)|^2\big|_{\Omega = \tau/k''z},$$

where $k'' = k_s'' + k_i''$. As in the case of a short pulse, the width of the correlation function after passing through the dispersion medium of length z becomes $\tau = 2\pi z k''/\tau_0$, where τ_0 is its initial width. Therefore, if the initial width of the second-order correlation function is 50 fs, its width becomes equal to 6 ns after passing two-photon light through an optical fiber 1 km in length (it is assumed that k'' for the fiber equals 3×10^{-28} s^2/cm [4]). As for the shape of the correlation function, it coincides with the spectrum given by Eq. (2). Such a two-photon wave packet in the far zone can be called *a two-photon spectron.*

The smearing of the biphoton correlation function in a dispersion medium should necessarily be taken into account when designing the schemes of quantum information transmission by two-photon light. It should be noted that this smearing in optical fibers can be compensated using the known linear methods of pulse compression [5] (the nonlinear methods are unsuitable because of the low intensity of biphoton fields). One sometimes assumes erroneously that the shape of the second-order correlation function for biphoton light manifests itself in the so-called anticorrelation effect [7], which consists of a sharp decrease (practically to zero) in the number of coinciding photocounts of two detectors, which detect both signal and idler beams (before detection, the signal and idler beams impinge on a beam splitter, so that the effect can only be observed if the optical paths of the signal and idler photons are balanced before beam splitting). However, it is known that the presence of a dispersion medium, through which the signal and idler beams propagate before beam splitting, has no effect on the shape of the anticorrelation "dip" [7]. This effect can easily be explained if one considers that the dip shape is associated not with the second-order but with the first-order correlation function [8]. However, according to Eq. (3), the propagation of two-photon light (as well as any other radiation) in a transparent medium with group velocity dispersion does not affect the shape of the first-order correlation function.

REFERENCES

1. D. N. Klyshko, *Photons and Nonlinear Optics* (Nauka, Moscow, 1980).

2. K. Mattle, H. Weinfurter, P. G. Kwiat, and A. Zeilinger, Phys. Rev. Lett. **76**, 4656 (1996).

3. A. V. Belinsky and D. N. Klyshko, Laser Phys. **4**, 663 (1994).

4. S. A. Akhmanov and S. Yu. Nikitin, *Physical Optics* (Mosk. Gos. Univ., Moscow, 1998).

5. S. A. Akhmanov, V. A. Vysloukh, and A. S. Chirkin, *The Optics of Femtosecond Pulses* (Nauka, Moscow, 1988).

6. C. K. Hong, Z. Y. Ou, and L. Mandel, Phys. Rev. Lett. **59**, 2044 (1987); Y. H. Shih and C. O. Alley, Phys. Rev. Lett. **61**, 2921 (1988).

7. A. M. Steinberg, P. G. Kwiat, and R. Y. Chiao, Phys. Rev. Lett. **68**, 2421 (1992).

8. A. V. Burlakov, M. V. Chekhova, O. A. Karabutova, and S. P. Kulik, Phys. Rev. A **64**, 041803 (2001).

Translated by V. Sakun

Generation of Compressed Sub-Poisson Bose Condensate by an Atom Laser

A. V. Kozlovskiĭ and A. N. Oraevskiĭ

Lebedev Physical Institute, Russian Academy of Sciences, Leninskiĭ pr. 53, Moscow, 119991 Russia
Received January 11, 2002; in final form February 13, 2002

The dynamics of Bose-condensate generation by a cw atom laser with simultaneous stimulated evaporative cooling in a magnetic trap was analyzed using a quantum-mechanical master equation. The model of the atom laser includes irreversible processes of incoherent trap mode pumping and spontaneous atomic transitions due to the interaction of the atomic ensemble with heat reservoirs. The inelastic atomic collisions in the trap and the continual coherent Bose-condensate output coupling from the trap were considered. At certain values of parameters, the Bose condensate created in this laser scheme occurs in a compressed sub-Poisson state. For large Bose condensates with a mean number of atoms $\sim 10^6$, the Fano factor may be as high as $\cong 0.5$. The influence of spontaneous transitions from the excited trap modes on the statistics of Bose condensate was analyzed. © *2002 MAIK "Nauka/Interperiodica".*

PACS numbers: 03.75.Fi; 32.80.Pj; 42.50.Ct

Recent successful experiments on the creation of atomic Bose condensates in traps have opened up possibilities of designing coherent sources of matter waves (atom lasers) [1, 2]. The fundamental property of a laser is that it creates a coherent field. The coherence and quantum-statistical properties of this field are the subject of investigations in the quantum optics of photon and atomic fields [3–9, 19]. The existing phenomenological semiclassical theories [10–15] and the quantum-mechanical theories [3–9, 16–27] devoted to studying atom lasers with various schemes of pumping, cooling, and field outcoupling from the trap predict the presence of a lasing threshold, saturation, as well as a high degree of coherence for the Bose condensate generated by an atom laser.

We consider an open atomic system confined in a trap and, therefore, having discrete energy levels. The trapped atoms in the respective electronic states interact with a set of reservoirs (bathes) formed by groups of untrapped atoms, which render pumping of the trap states incoherent because of the transitions of pump-reservoir atoms to the electronic states in which they are captured by the trap field. Such a reservoir is also responsible for the trap losses caused by the backward electronic transitions. The coherent Bose-condensate output coupling from the trap is provided by the interaction of the lowest trap state with the continuum reservoir (vacuum). In the evaporative cooling model considered in this work, the upper excited states of the trap are intensely depleted due to the interaction with the rf electromagnetic field. The interaction of the trapped atoms with the phonon field of a continuum atomic reservoir is considered as a source of spontaneous transitions between the discrete atomic states in the trap (see also [26, 27]).

To describe the system of trapped atoms interacting with reservoirs, we use the formalism of secondary quantization for atomic fields and introduce the creation and annihilation operators of the form

$$\Psi_S(\mathbf{r}) = \sum_j a_j \phi_j(\mathbf{r}), \quad a_j = \int d^3 \mathbf{r} \phi_j^*(\mathbf{r}) \Psi_s(\mathbf{r}), \quad (1)$$

$$\Psi_\alpha(\mathbf{r}) = \sum_{\lambda=0}^{\infty} b_{\alpha\lambda} \psi_{\alpha\lambda}(\mathbf{r}),$$

$$b_{\alpha\lambda} = \int d^3 \mathbf{r} \psi_{a\lambda}^*(\mathbf{r}) \Psi_\alpha(\mathbf{r}), \quad \alpha = p, \text{out}, sp, \tag{2}$$

where $\Psi_s^{(+)}(\mathbf{r})$ is the operator of annihilation (creation) of an atom in the trap at the point $\mathbf{r}$, and $\Psi_\alpha^{(+)}(\mathbf{r})$ are the operators of (p) annihilation (creation) of the pump reservoirs, (out) coherent atomic-field outcoupling, and (sp) spontaneous radiation. These operators obey the following commutation relations:

$$[\Psi_\alpha(\mathbf{r}), \Psi_{\alpha'}^{(+)}(\mathbf{r}')] = \delta_{\alpha,\alpha'} \delta(\mathbf{r}-\mathbf{r}'),$$
$$\alpha, \alpha' = S, p, \text{out}, sp, \tag{3}$$
$$[\Psi_\alpha(\mathbf{r}), \Psi_{\alpha'}(\mathbf{r})] = [\Psi_{\alpha'}^{(+)}(\mathbf{r}), \Psi_{\alpha'}^{(+)}(\mathbf{r}')] = 0.$$

In terms of field operators (1) and (2), the effective one-particle Hamiltonian containing the free-energy terms and the operators of interaction between the system and the reservoirs

$$H = H_0 + \sum_0 H_{R\alpha} + \sum_\alpha V_{R\alpha,S} + V_{\text{coll}} \tag{4}$$

can be recast as

$$H = \sum_j \hbar\omega_j a_j^+ a_j + \sum_\alpha \sum_{\lambda=0} \hbar\omega_{\alpha\lambda} b_{\alpha\lambda}^+ b_{\alpha\lambda}$$

$$+ \sum_{\lambda=0}^\infty \left\{ \sum_{i>j} \hbar(\Gamma_{\lambda,i,j} b_{sp,\lambda}^+ a_i a_j^+ + \text{h.c.}) \right.$$

$$+ \sum_i \hbar(\kappa_{\lambda,i} b_{p,\lambda} a_i^+ + \text{h.c.}) \tag{5}$$

$$\left. + \sum_i \hbar(\mu_{\lambda,i} b_{\text{out},\lambda}^+ a_i + \text{h.c.}) \right\}$$

$$+ \frac{1}{2} \sum_j \hbar(g_{i,j,k,l} a_i^+ a_j^+ a_k a_1 + \text{h.c.})_{i,j,k,l}.$$

The first two terms in Eqs. (4) and (5) are the atomic energy in the trap and the self-energy of reservoir oscillators, respectively. The next three terms in Eq. (5) [$V_{R\alpha S}$ in Eq. (4)] are the sum of potentials of interaction between the trapped atoms (system) and the reservoirs responsible for the dissipation, pumping, and spontaneous decay from the discrete energy levels of the trap. The coupling constants of the system to these reservoirs are denoted by μ, κ, and Γ, respectively. The last term (V_{coll}) is the interaction potential for the elastic and inelastic binary collisions of the trapped atoms.

In this work, we consider an atom laser model with evaporative atom cooling [1, 2]. The preliminary cooled atoms enter the trap formed by the thermodynamically equilibrium reservoirs. The atoms in the trap are in four energy states characterized by the creation (annihilation) operators a_i^+ (a_i), where $i = 0$, 1, 2, and 3. It is also assumed that the high-lying trap levels are sparsely populated because of the stimulated evaporation mechanism implemented by the rf electromagnetic field applied to the trap [1]. The Bose condensate achieves its lowest energy state a_0^+ (a_0), from which the accumulated condensate exits with the rate κ_{out} to the continuum reservoir of vacuum states (laser output radiation). Various methods of the exit trap were considered for Bose condensate in [11, 24]. Pumping of each of the trap states is accomplished independently, with rates p_i from the corresponding individual reservoirs having mean occupation numbers N_i, and the rates of backward dissipation processes from the trap are γ_i. The problem of pumping an atom laser from the thermal bathes was considered in [5, 21–23].

In the case of binary collisions between the trapped atoms, the interaction energy of colliding atoms [the last term in Eq. (5)] contains the following terms in the dipolar approximation:

$$V_{\text{coll}} = V_{\text{elast}} + V_{\text{inelast}},$$

$$V_{\text{elast}} = V_{jj} + V_{ij} \tag{6}$$

$$= \sum_{j=0}^3 \hbar g_{jjjj} a_j^{+2} a_j^2 + \sum_{i,j=0,\ i<j}^3 \hbar g_{ijij} a_i^+ a_j^+ a_i a_j,$$

$$V_{\text{inelast}} = \hbar g_{0211} a_0^+ a_2^+ a_1^2 + \hbar g_{1102} a_1^{+2} a_0 a_2$$

$$+ \hbar g_{0312} a_1 a_2 a_3^+ a_0^+ + \hbar g_{1203} a_0 a_3 a_1^+ a_2^+ \tag{7}$$

$$+ \hbar g_{1322} a_1^+ a_3^+ a_2^2 + \hbar g_{2213} a_2^{+2} a_1 a_3,$$

where $g_{ijkl} = g_{klij}^*$.

Eliminating the bath variables by the standard procedure, one obtains, in the Born and Markovian approximations, the master equation for the reduced density operator of the system. The presence of reservoirs gives rise to the terms accounting for the dissipative processes, field outcoupling from the trap, pumping, and spontaneous decay in the equation of motion.

Since all operators in Hamiltonian (7) are bilinear in the creation and annihilation operators, the contribution to the coherent (unitary) evolution of the diagonal matrix elements is zero. All elastic collisions have a dispersive character and influence the time evolution of the off-diagonal matrix elements and, hence, determine the magnitude of first-order field coherence.

Assuming that the rates of atom outcoupling from the upper states are high for the density operator, one can eliminate adiabatically the $|2\rangle$ and $|3\rangle$ modes. The resulting master equation for the irreversible processes can be written as

$$\dot{\rho}\big|_{\text{irr}} = \left\{ \frac{\kappa_{\text{out}} + \gamma_0(\bar{N}_0 + 1)}{2} D[a_0] + \frac{p_0}{2}\bar{N}_0 D[a_0^+] \right.$$

$$+ \frac{\gamma_1}{2}(\bar{N}_1 + 1)D[a_1] + \frac{p_1}{2}\bar{N}_1 D[a_1^+]$$

$$+ \frac{\gamma_{sp}}{2}\{(\bar{N}_{01} + 1)D[a_0^+ a_1] + \bar{N}_{01}D[a_1^+ a_0]\} \tag{8}$$

$$\left. + \frac{\Omega_1}{2} D[a_0^+ a_1^2] + \frac{\Omega_2}{2}[a_0^{+2} a_1^3] \right\}\rho,$$

where $D[o]\rho \equiv 2o\rho o^+ - o^+ o\rho - \rho o^+ o$ for the corresponding operator o.

The quantity γ_{sp} is the spontaneous transition rate between the trap modes $|1\rangle$ and $|0\rangle$, $\bar{N}_{01} = \bar{N}(\omega_{sp,\lambda}) = \langle b_{sp,\lambda}^+, b_{sp,\lambda}\rangle$, and $\hbar\omega_{sp,\lambda} = \hbar(\omega_1 - \omega_0) = \hbar\omega_{01}$ is the mean number of phonons in the spontaneous-decay reservoir at the frequency of trap transition. Similarly, $\bar{N}_0$ and $\bar{N}_1$ are mean numbers of atoms in the reservoirs coupled to the states $|0\rangle$ and $|1\rangle$, respectively.

The effective inelastic collision rates in Eq. (8) are

$$\Omega_1 = \frac{4|g_{0211}|^2}{\gamma_2}, \quad \Omega_2 = \frac{16|g_{0211}|^2|g_{0312}|^2}{\gamma_2^2\gamma_3}. \quad (9)$$

We will assume below that the loss rates for the nonlaser field modes are much higher than the rates of pumping and coherent laser mode outcoupling, as well as of the effective evaporation rates; i.e., $\gamma_2, \gamma_3 \gg p_i, \kappa_{out}, \Omega_j, \gamma_{sp}$ for $i = 0, 1, 2, 3$ and $j = 1, 2$, thereby providing for the low populations of the $|2\rangle$ and $|3\rangle$ modes.

For the diagonal matrix elements of the reduced density matrix $\rho_{n_0 n_1}(t) \equiv \langle n_0 n_1|\rho(t)|n_0 n_1\rangle$, one has

$$\dot{\rho}_{n_0, n_1} = (\kappa_{out} + \gamma_0(\overline{N}_0 + 1))[(n_0 + 1)\rho_{n_0 + 1, n_1} - n_0\rho_{n_0 n_1}]$$

$$+ p_0\overline{N}_0[n_0\rho_{n_0 - 1, n_1} - (n_0 + 1)\rho_{n_0 n_1}]$$

$$+ \gamma_1(\overline{N}_1 + 1)[(n_1 + 1)\rho_{n_0, n_1 + 1} - n_1\rho_{n_0 n_1}]$$

$$+ p_1\overline{N}_1[n_1\rho_{n_0, n_1 - 1} - (n_1 + 1)\rho_{n_0 n_1}]$$

$$+ p_0\overline{N}_0[n_0\rho_{n_0 - 1, n_1} - (n_0 + 1)\rho_{n_0 n_1}]$$

$$+ \gamma_1(\overline{N}_1 + 1)[(n_1 + 1)\rho_{n_0, n_1 - 1} - n_1\rho_{n_0 n_1}]$$

$$+ \gamma_{sp}\{(\overline{N}_{01} + 1)[n_0(n_1 + 1)\rho_{n_0 - 1, n_1 + 1}$$

$$- n_1(n_0 + 1)\rho_{n_0 n_1}] + \overline{N}_{01}[n_1(n_0 - 1)\rho_{n_0 + 1, n_1 - 1}$$

$$- n_0(n_1 + 1)\rho_{n_0 n_1}]\} + \Omega_1[n_0(n_1 + 1)(n_1 + 2)\rho_{n_0 - 1, n_1 + 2}$$

$$- (n_0 + 1)(n_1 - 1)\rho_{n_0 n_1}]$$

$$+ \Omega_2[(n_0 - 1)n_0(n_1 + 1)(n_1 + 2)(n_1 + 3)\rho_{n_0 - 2, n_1 + 3}$$

$$- (n_0 + 2)(n_0 + 1)n_1(n_1 - 1)\rho_{n_0 n_1}]. \quad (10)$$

The quantum-mechanical means of the number of atoms in the lowest trap state (laser mode) and of the variance (fluctuation) of the number of atoms are calculated using the diagonal matrix elements of the density matrix according to the relationships

$$\langle n_{BC}(t)\rangle = sp(a_0^+a_0\rho(t)) = \sum_{n_0, n_1} n_0\rho_{n_0, n_1}(t), \quad (11)$$

$$\langle(\Delta n_i(t))^2\rangle \equiv Var n_i = sp(a_i^+a_ia_i^+a_i\rho(t)) - \langle n_i\rangle^2$$

$$= \sum_{n_0, n_1} (n_i - \langle n_i\rangle)^2\rho_{n_0 n_1}(t), \quad i = 0, 1. \quad (12)$$

The Fano factors for the Bose condensate and for the first excited state of the trap are defined as

$$F_i = \frac{(\langle\Delta n_i\rangle^2)}{\langle n_i\rangle}, \quad i = 0, 1. \quad (13)$$

In what follows, the pumping rates will be ignored for all modes except for $|2\rangle$; the atomic transitions from the laser mode $|0\rangle$ to the bath will also be ignored; i.e., we assume that the rate of Bose-condensate outcoupling from the lowest trap state into the vacuum is κ_{out}. The influence of the $|3\rangle$ mode will also be ignored; i.e., it is assumed that $\Omega_2 \ll \kappa_{out}$.

In the laser model considered in this work, the dynamics of atomic-field generation depends qualitatively on the ratios between the pumping rate (p_1) into the state $|1\rangle$ of the atomic trap and the rates (κ_{out}) of Bose-condensate outcoupling from the lowest state $|0\rangle$, (Ω_1) of induced transitions from the state $|1\rangle$ to the states $|0\rangle$ and $|2\rangle$, and (γ_{sp}) of spontaneous transition to the state $|0\rangle$ from the state $|1\rangle$ due to the interaction with the bath. Assuming that γ_1 is much less than all these rates, the generation regimes of the atom laser can be divided into two characteristic types. If $p_1 > \Omega_1$ and p_1, $\Omega_1 \sim \kappa_{out}$, then two stages can be distinguished in the lasing dynamics (Figs. 1a, 1b): the state $|1\rangle$ is populated first. In the slowly growing Bose condensate, the number of particles in the state $|0\rangle$ is small, and the fluctuations of the number of particles rapidly increases to the values $\langle(\Delta n_{BC})^2\rangle = (\langle n_0\rangle + 1)\langle n_0\rangle$ typical of a chaotic heat field. At the second stage, the number of atoms $\langle n_1\rangle$ decreases and $\langle n_0\rangle$ increases with the simultaneous decrease in the fluctuation $\langle(\Delta n_0)^2\rangle$ to achieve the Poisson value $\langle n_0\rangle_{ss}$ in the steady state. If $p_1 > \Omega_1$ and p_1, $\Omega_1 \gg \kappa_{out}$, the steady-state Bose condensate in the state $|0\rangle$ may occur in the compressed sub-Poisson state $F_0 < 1$ with an insignificant compression (Fig. 1c).

If $p_1 \ll \Omega_1$ and p_1, $\Omega_1 \gg \kappa_{out}$, the regime of Bose-condensate generation becomes cardinally different (Fig. 2). The population stage is absent for $|1\rangle$ in the lasing dynamics, and a sharp growth of the Bose-condensate fluctuations in the state $|0\rangle$ is also absent. The Bose-condensate fluctuations may attain sub-Poisson magnitudes of the compressed state (Fig. 2a). The population $|1\rangle$ of the state $|1\rangle$ is small at all times up to the establishing of the steady state, and the fluctuations $\langle(\Delta n_1)^2\rangle$ of the number of particles become of the essentially sub-Poisson: $F_1 < 1$. In the regime p_1, $\Omega_1 \gg \kappa_{out}$, the population $\langle n_1\rangle_{ss}$ is equal to 0.333 and the variance of the number of particles $\langle(\Delta n_1)^2\rangle_{ss} = 0.667\langle n_1\rangle_{ss}$ irrespective of the transition rates (Fig. 2b).

Our systematic numerical calculations showed that the conditions for creating Bose condensate in the compressed sub-Poisson state amount to the inequalities $\Omega_1 \gg p_1 \gg \kappa_{out} \gg \gamma_1$, irrespective of $\overline{N}_1$. The degree of compression increases with an increase in the number of bosons in the condensate, $\langle n_0\rangle_{ss} \gg 1$, if $\Omega_1, p_1 \gg \kappa_{out}$. For the laser parameters satisfying the relationships $\Omega_1 \gg p_1 \gg \kappa_{out} \gg \gamma_1$, for which $\langle n_0\rangle_{ss} \sim 10^6$, the maximal fluctuation suppression is almost twice the shot noise level, and the Fano factor attains the value $F_{0, ss} \approx 0.54$ (Fig. 2a).
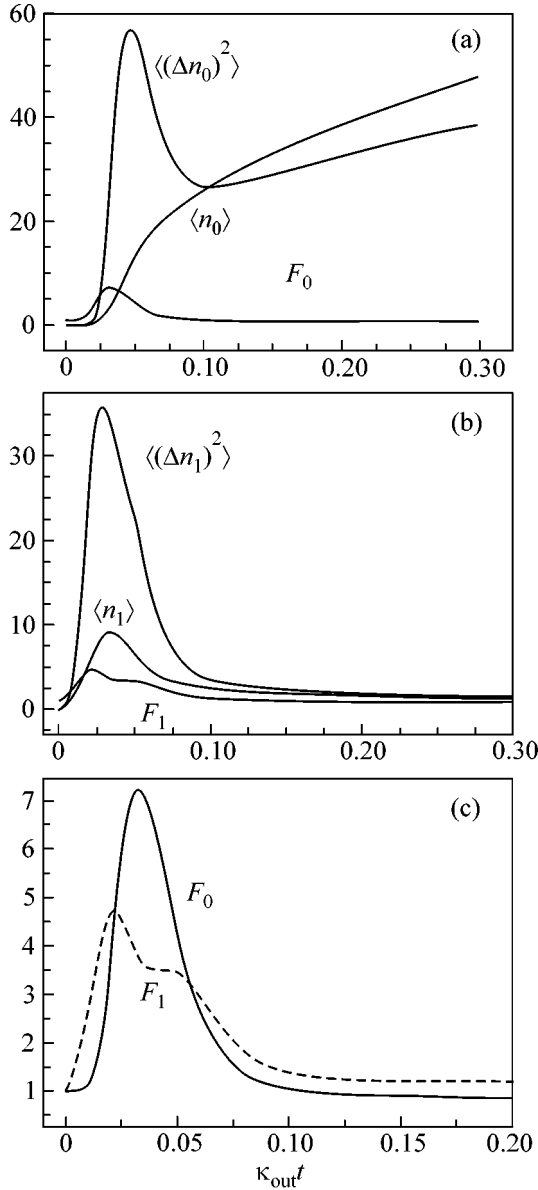
Fig. 1. (a) The mean number $\langle n_0 \rangle$ of atoms in the Bose condensate, the variance (fluctuation) $\langle (\Delta n_0)^2 \rangle$ of the number of atoms, and the Fano factor $F_0 = \langle (\Delta n_0)^2 \rangle / \langle n_0 \rangle$ as functions of the reduced time $\kappa_{out} t$ for the pumping rate $p_1 = 100 \kappa_{out}$, collision transition rate $\Omega_1 = \kappa_{out}$, mean number of particles in the bath $\bar{N}_1 = 1$, and $\gamma_{sp} \ll \Omega_1$. (b) Time evolution of the quantities $\langle n_1 \rangle$, $\langle (\Delta n_1)^2 \rangle$, and $F_1 = \langle (\Delta n_1)^2 \rangle / \langle n_1 \rangle$ for the first excited state in the trap and for the parameters used in (a). (c) Time evolution of the Fano factors F_0 and F_1 for the parameters used in (a).

Fig. 2. (a) Time evolution of the Fano factor for $p_1 = 10^6 \kappa_{out}$, $\Omega_1 = 10^9 \kappa_{out}$, $\bar{N} = 1$, and $\gamma_{sp} \ll \kappa_{out}$. (b) Time evolution of $\langle n_1 \rangle$, $\langle (\Delta n_1)^2 \rangle$, and F_1 for the parameters given in (a): $\Omega_1 \gg p_1 \gg \kappa_{out} \gg \gamma_{sp}$. (c) Time evolution of $\langle n_0 \rangle$ and $\langle (\Delta n_0)^2 \rangle$ for the parameters given in (a).

Computations showed that, at $p_1 \gg \bar{N}_1 \gg \Omega_1$ and $p_1 \bar{N}_1 \kappa \gg \kappa_{out} \gg \gamma_1$, the steady-state mean number of atoms in the Bose condensate can be estimated from the formula

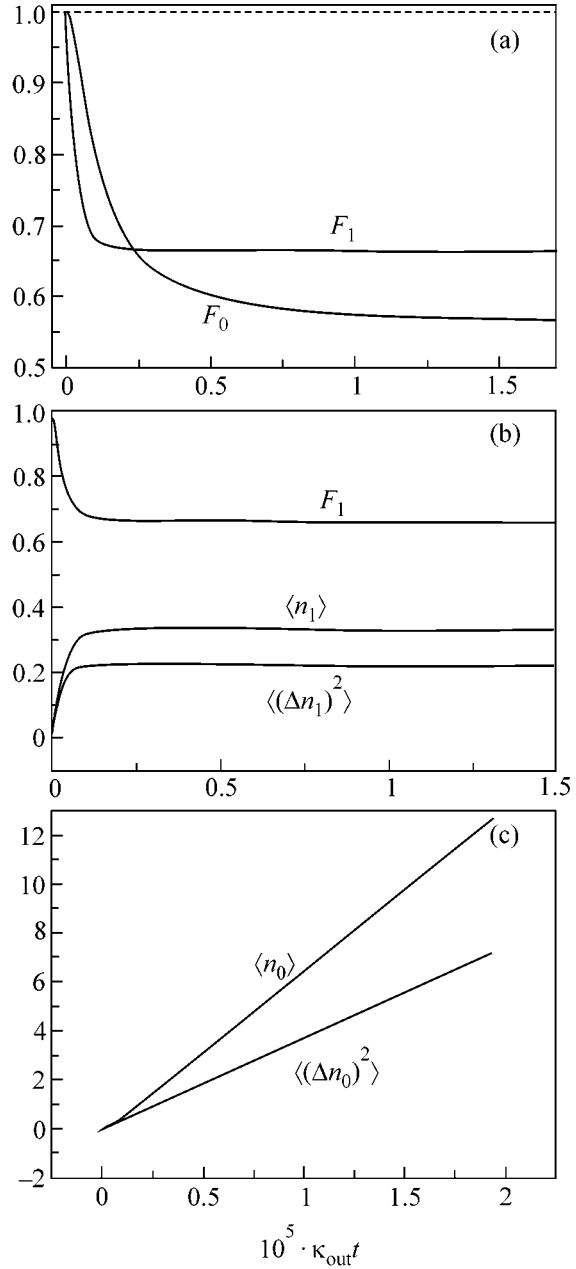$$\langle n_0 \rangle_{ss} \approx \frac{p_1}{2\kappa_{out}} \left(\bar{N}_1 - \frac{1}{2} + \left(\frac{1}{4} + \frac{\kappa_{out}}{\Omega_1} \right)^{1/2} \right). \qquad (14)$$

In [7], where the atom laser model was analogous to ours, the master equation for the density operator was

transformed to the Fokker–Planck equation for the quasiprobability P in the phase space of atomic-field amplitude and phase. This equation was used in [7] to derive the stochastic differential equations for the number of particles and field phases in the trap modes and then solved for the mean values under the steady-state conditions. In the limit $n_0 \gg 1$, the semiclassical expression for the mean number of atoms in the lowest trap state was found in [7, 25] in the form analogous to Eq. (14), but the square-root sign, which was arbitrary in those calculations, was chosen to be negative. Our exact quantum-mechanical calculations indicate that Eq. (14) with the positive root sign is valid with a high accuracy.

The calculations also showed that, at $p_1 \sim \bar{N}_1 \, \Omega_1$, the mean number of atoms in the Bose condensate is described by the formula $\eta p_1 \bar{N}_1 \kappa_{\text{out}}$, where $\eta \cong 2$. This relation is qualitatively consistent with the computational results obtained for the analogous laser scheme in [3]; namely, $\langle n_0 \rangle = 2 p_1 \bar{N}_1 / 3 \kappa_{\text{out}}$ for the case considered in this work, i.e., for $\Omega_1 > p_1 \bar{N}_1 \gg \kappa_{\text{out}}$.

The lasing threshold in our case is expressed as $p_1 \bar{N}_1 > \kappa_{\text{out}}$.

It is assumed in the above computations that the spontaneous transition rates between the trap modes are much lower than the rates of other processes. The calculations carried out for the situation where the spontaneous transition rates are comparable with the rate of coherent condensate output coupling from the trap, i.e., for $\gamma_{sp} = 0.5 \kappa_{\text{out}}$ and $\bar{N}_{01} = 1$, are presented in Fig. 3. A comparison of the values characterizing the condensate under these conditions with the values in the absence of spontaneous decay ($\gamma_{sp} \ll \kappa_{\text{out}}$) indicates that the spontaneous transitions have no effect on the steady-state mean $\langle n_0 \rangle_{ss}$ but considerably enhance the Bose-condensate fluctuations $\langle (\Delta n_0)^2 \rangle_{ss}$ and alter the evolution dynamics for the atom laser action.

The quantum-mechanical calculations performed in this work suggest that the evaporative continuous-wave atom laser allows the creation of both the Bose microcondensate with the mean number of particles $\langle n_0 \rangle \sim 10$ and the Bose macrocondensate with $\langle n_0 \rangle \sim 10^6$ in the compressed sub-Poisson state. However, the fluctuation of the number of particles in the microcondensate deviates only slightly from the Poisson distribution, whereas the compression for the macrocondensate is large and is almost twofold (Fano factor $F_{\text{BC}} \longrightarrow 0.5$). The condition for the generation of the compressed Bose condensate amounts to the requirement that the rate of coherent atomic-field outcoupling from the trap and the rate of spontaneous transitions between the trap modes be smaller than the rates of incoherent pumping and induced transitions caused by the atomic collisions in the trap. The results obtained in this work allow the assumption to be made that one may construct schemes
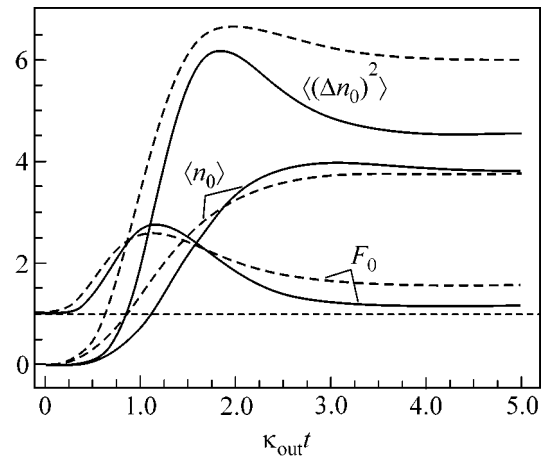
Fig. 3. Influence of spontaneous transitions on atom laser dynamics. The solid lines correspond to the Bose condensate with the following parameters of spontaneous transitions: $\gamma_{sp} = 0.5 \kappa_{\text{out}}$ and $\bar{N}_{01} = 1$. The dashed lines are the same for $\gamma_{sp} = 0.001 \kappa_{\text{out}}$ and $\bar{N}_{01} = 0.001$. The remaining parameters are $p_1 = 2 \kappa_{\text{out}}$, $\Omega_1 = 0.1 \kappa_{\text{out}}$, and $\bar{N} = 1$.

of atom lasers which are capable of generating relatively small Bose condensates in the states close to the Fock state. Such lasers can be considered as sources of groups of ultracold atoms with a predetermined exact number of particles, which are necessary for some modern experiments in atomic and photon optics.

REFERENCES

1. I. Bloch, T. W. Hansch, and T. Esslinger, Phys. Rev. Lett. **82**, 3008 (1999).
2. M.-O. Mewes, M. R. Andrews, D. M. Kurn, *et al.*, Phys. Rev. Lett. **78**, 582 (1997).
3. M. Holland, K. Burnett, C. Gardiner, *et al.*, Phys. Rev. A **54**, R1757 (1996).
4. M. Guzman, M. Moore, and P. Meystre, Phys. Rev. A **53**, 977 (1996).
5. M. J. Steel, M. K. Olsen, L. I. Plimak, *et al.*, Phys. Rev. A **58**, 4824 (1998).
6. M. J. Moore and P. Meystre, Phys. Rev. A **56**, 2989 (1997).
7. O. Zobay and P. Meystre, Phys. Rev. A **57**, 4710 (1998).
8. E. V. Goldstein, O. Zobay, and P. Meystre, Phys. Rev. A **58**, 2373 (1998).
9. H. M. Wiseman, A. Martin, and D. F. Walls, Quantum Semiclassic. Opt. **8**, 737 (1996).
10. R. J. C. Spreew, T. Pfau, and M. Wilkens, Europhys. Lett. **32**, 469 (1995).
11. G. M. Moy, J. J. Hope, and C. M. Savage, Phys. Rev. A **55**, 3631 (1997).
12. A. H. Oraevskiĭ, Zh. Éksp. Teor. Fiz. **103**, 981 (1993) [JETP **76**, 480 (1993)].
13. A. Imamoglu, R. J. Ram, S. Pau, and Y. Yamamoto, Phys. Rev. A **53**, 4250 (1996).

14. L. N. Oraevskiĭ, Kvantovaya Élektron. (Moscow) **24**, 1127 (1997).

15. V. Kneer, T. Wang, K. Vogel, *et al.*, Phys. Rev. A **58**, 4841 (1998).

16. H. M. Wiseman and M. J. Collett, Phys. Lett. A **202**, 246 (1995).

17. Ch. J. Borde, Phys. Lett. A **204**, 217 (1995).

18. U. Janicke and H. Wilkens, Europhys. Lett. **35**, 561 (1996).

19. H. M. Wiseman, Phys. Rev. A **56**, 2068 (1997).

20. R. Quadt, H. M. Wiseman, and D. F. Walls, Phys. Lett. A **219**, 19 (1996).

21. M. J. Steel and D. F. Walls, Phys. Rev. A **56**, 3832 (1997).

22. J. I. Cirac and M. Lewenstein, Phys. Rev. A **53**, 2466 (1996).

23. C. M. Savage, J. R. Roustekovski, and D. F. Walls, Phys. Rev. A **57**, 3805 (1998).

24. G. M. Moy, J. J. Hope, and C. M. Savage, Phys. Rev. A **59**, 667 (1999).

25. H. P. Breuer, D. Fallen, and B. Kappler, Phys. Rev. A **60**, 3188 (1999).

26. M. O. Scully, Phys. Rev. Lett. **82**, 3927 (1999).

27. V. V. Kocharovsky, M. O. Scully, S.-Y. Zhu, and M. S. Zubairy, Phys. Rev. A **61**, 023609 (2000).

Translated by V. Sakun

Phase Separation and Vortex States in Binary Mixture of Bose–Einstein Condensates in Trapping Potentials with Displaced Centers[1]

S. T. Chui[1], V. N. Ryzhov[2, *], and E. E. Tareyeva[2]

[1] *Bartol Research Institute, University of Delaware, Newark, DE 19716*
[2] *Institute for High Pressure Physics, Russian Academy of Sciences,*
Troitsk, Moscow region, 142190 Russia
* *e-mail: ryzhov@hppi.troitsk.ru*
Received January 28, 2002

A system of two simultaneously trapped condensates consisting of ^{87}Rb atoms in two different hyperfine states is investigated theoretically in the case where the minima of the trapping potentials are displaced with respect to each other. It is shown that the small shift of the minima of the trapping potentials leads to a considerable displacement of the centers of mass of the condensates, in agreement with the experiment. It is also shown that the critical angular velocities of the vortex states of the system drastically depend on the shift and the relative number of particles in the condensates, and there is a possibility to exchange the vortex states between condensates by shifting the centers of the trapping potentials. © 2002 MAIK "Nauka/Interperiodica".

PACS numbers: 03.75.Fi, 47.32.Cc

The experimental realization of Bose–Einstein Condensation (BEC) in trapped alkali-atoms gases at ultralow temperatures offers new opportunities for studying quantum degenerate fluids [1–3]. The art of manipulating these condensates, which contain thousands of atoms confined to microscale clouds, has now achieved a very high level. Creation of vortices in one [4] and two-component BEC [5, 6] of ^{87}Rb atoms is an amazing example of this art.

In this article, we focus on the properties of the two-component BEC in the trap, in which the trapping potentials for each component are displaced with respect to each other in the vertical direction [7]. The condensate consists of simultaneously trapped otherwise identical atoms of ^{87}Rb in two different hyperfine spin states $|1\rangle$ and $|2\rangle$ ($|1\rangle$ and $|2\rangle$ denote the $|F = 1, m_f = -1\rangle$ and $|2\rangle$, $|1\rangle$ spin states of ^{87}Rb atoms, respectively) [7–9]. The scattering lengths of the states $|1\rangle$ and $|2\rangle$ are known to be in proportion $a_{11} : a_{12} : a_{22} = 1.03 : 1.0 : 0.97$, with the average of the three being 55(3) Å [7–9].

The double condensate system was prepared from the single $|1\rangle$ condensate by driving a two-photon transition, which transfers any desired fraction of the atoms to the $|2\rangle$ state by selecting the length and amplitude of the two-photon pulse [8]. The rotating magnetic field of the time-averaged orbiting potential trap gave the possibility of displacing the minima of the trapping potentials V_1 and V_2 with respect to each other. When the

minima of the trapping potentials were not shifted, the $|1\rangle$ atoms formed a shell about the $|2\rangle$ atoms [7]. This case was discussed theoretically in [10, 11]. If the minima of the trapping potentials V_1 and V_2 are displaced from each other by a distance which is small compared to the size of the total condensate, the resulting separation of the centers of mass of the condensates is much larger [7]. In this paper, we provide an analytical explanation of this result.

In order to explore the boundary between the two condensates, we begin with an analysis of their behavior in the framework of the Thomas–Fermi Approximation (TFA), which ignores the kinetic energy terms in the Gross–Pitaevskii equations for the condensate wave functions [12]. It has been shown that, in the case of one-component condensates, the TFA results agree well with the numerical calculations for large particle numbers, except for a small region near the boundary of the condensate [13, 14]. In fact, even for small numbers of particles, TFA still usually gives qualitatively correct results.

In the dimensionless variables, the Gross–Pitaevskii equations for the condensates in the harmonic traps may be written in the following form [10, 11]:

$$
-\nabla'^2 \psi_1' + (x'^2 + y'^2 + \lambda^2(z' + z_0')^2)\psi_1'
$$
$$
-\mu_1'\psi_1' + u_1|\psi_1'|^2\psi_1' + \frac{8\pi a_{12}N_2}{a_\perp}|\psi_2'|^2\psi_1' = 0; \tag{1}
$$

---

[1] This article was submitted by the authors in English.

$$-\beta^2 \nabla'^2 \psi_2' + (x'^2 + y'^2 + \lambda^2(z' - z_0')^2)\psi_2'$$

$$-\mu_2' \psi_2' + u_2 \beta^2 |\psi_2'|^2 \psi_2' + \frac{8\pi a_{12} N_1}{a_\perp} |\psi_1'|^2 \psi_2' = 0. \tag{2}$$

Here, $\psi_i(\mathbf{r}) = \sqrt{N_i/a_\perp^3}\,\psi_i'(\mathbf{r}')$; $\psi_i(\mathbf{r})$ is the wave function of the species i of a two-species condensate ($i = 1, 2$); $\lambda = \omega_z/\omega$; $\mathbf{r} = a_\perp \mathbf{r}'$, where $a_\perp = (\hbar/m\omega)^{1/2}$, ω is the trapping frequency; and $\mu_i' = 2\mu_i/\hbar\omega$, where μ_i is the chemical potential of the species i. The chemical potentials μ_1 and μ_2 are determined by the relations $\int d^3 |\psi_i|^2 = N_i$, and u_i is given by $u_i = 8\pi a_{ii} N_i/a_\perp$. The wave function $\psi_i'(\mathbf{r}')$ is normalized to 1, and z_0' denotes the shift of the minimum of the trapping potential in the vertical direction.

Equations (1) and (2) were obtained by minimization of the energy functional of the trapped bosons given by

$$E' = \frac{1}{2}\int d^3 r' \left[N_1 |\nabla' \psi_1'|^2 + N_2 \beta^2 |\nabla' \psi_2'|^2 \right.$$

$$+ N_1 (x'^2 + y'^2 + \lambda^2 (z' + z_0')^2)|\psi_1'|^2 + \frac{1}{2} N_1 u_1 |\psi_1'|^4$$

$$+ N_2 (x'^2 + y'^2 + \lambda^2 (z' - z_0')^2)|\psi_2'|^2 \tag{3}$$

$$\left. + \frac{1}{2} N_2 u_2 \beta^2 |\psi_2'|^4 + \frac{4\pi a_{12}}{a_\perp} N_1 N_2 |\psi_1'|^2 |\psi_2'|^2 \right].$$

Here, the energy of the system E is related to E' by $E = \hbar\omega E'$

In the TFA, Eqs. (1), (2), and (3) can be further simplified by omitting the kinetic energy terms. In the framework of TFA, the phase-segregated condensates do not overlap, so we can neglect the last terms in Eqs. (1), (2), and (3), obtaining simple algebraic equations

$$|\psi_1'(\mathbf{r}')|^2 = \frac{1}{u_1}(\mu_1' - (r'^2 + \lambda^2(z' + z_0')^2))$$

$$\times \Theta(\mu_1' - (r'^2 + \lambda^2(z' + z_0')^2)) \tag{4}$$

$$\times \Theta(r'^2 + \lambda^2(z' - z_0')^2 - \mu_2');$$

$$|\psi_2'(\mathbf{r}')|^2 = \frac{1}{u_2}(\mu_2' - (r'^2 + \lambda^2(z' - z_0')^2))$$

$$\times \Theta(\mu_2' - (r'^2 + \lambda^2(z' - z_0')^2)) \tag{5}$$

$$\times \Theta(r'^2 + \lambda^2(z' + z_0')^2 - \mu_1').$$

Here, Θ denotes the unit step function and $\rho'^2 = x'^2 + y'^2$. If $z_0' = 0$, from Eqs. (4) and (5) one can see that the con-

densate density has the ellipsoidal form. This case was considered in detail in [10, 11].

In the case of phase separation, the energy of the system can be written in the form [10, 11] $E = E_1 + E_2$, where

$$E_1 = \frac{1}{2}\hbar\omega N_1 \left[\mu_1' - \frac{1}{2}u_1 \int d^3 r' |\psi_1'|^4 \right], \tag{6}$$

$$E_2 = \frac{1}{2}\hbar\omega N_2 \left[\mu_2' - \frac{1}{2}u_2 \int d^3 r' |\psi_2'|^4 \right]. \tag{7}$$

To determine the position of the boundary between the condensates, we use the condition of thermodynamic equilibrium [15]: the pressures exerted by both condensates must be equal, $P_1 = P_2$. Pressure is given by [16]: $P_i = G_{ii}|\psi_i|^4/2$, where $G_{ii} = 4\pi\hbar 2 a_{ii}/m_i$. Using these equations, one can obtain the equation for the phase boundary

$$r''^2 + \left(\lambda z'' - \frac{\alpha(\kappa + 1)}{\kappa - 1} \right)^2 = R^2, \tag{8}$$

where $z' = \sqrt{\mu_1'}\,z''$, $r' = \sqrt{\mu_1'}\,r''$, $r'^2 = x'^2 + y'^2$, $\alpha = \lambda z_0''$, $\kappa = \sqrt{a_{11}/a_{22}}$, and

$$R^2 = \frac{\mu_1' - \kappa\mu_2'}{\mu_1'(1 - \kappa)} + \frac{4\alpha^2 \kappa}{(\kappa - 1)^2}. \tag{9}$$

From Eqs. (8) and (9) one can easily understand why a small displacement of the centers of the trapping potentials leads to the significant separation of the centers of mass of the condensates [7]. The basic physics of this amplification of the trap center difference comes from the two possible final configurations of the mixture and from the fact that the system is close to the "critical point" that separates the two final configurations. Of the two configurations, one is symmetric, where one component is inside and the other component is outside, and another is asymmetric [17–19], where the two components are on the opposite sides.

The former configuration is favorable if $\kappa = \sqrt{a_{11}/a_{22}}$ is different from unity, with the less repulsive component being in the middle, where the density is higher. The asymmetric configuration possesses a lower interface energy and is favorable when κ is close to unity. We found that in the Thomas–Fermi approximation, when the trapping frequencies for the two components are the same, the amplification factor is proportional to $1/(\kappa - 1)$.

From Eqs. (8), (9) the evolution of the system upon increasing α may be described as follows: for $\alpha = 0$, condensate 1 forms the shell about the ellipsoidal condensate 2. The semiaxis of this ellipsoid is given by Eq. (8) for $\alpha = 0$. Upon increasing α, the inner ellipsoid moves upwards, while the external one moves down.

It may be shown that they touch each other at the critical value of α: $\alpha_c = \frac{1}{2}(1 - \sqrt{\mu_2'/\mu_1'})$. For $\alpha > \alpha_c$, phase boundary (8) intersects boundaries of condensates at the points with coordinates

$$\lambda z_c'' = \frac{\alpha}{\kappa - 1} - \frac{(\kappa - 1)(R^2 - 1)}{4\alpha\kappa}, \qquad (10)$$

$$r_{1,2}'' = \pm\sqrt{1 - (\lambda z_c'' + \alpha)^2}, \qquad (11)$$

which can be obtained from Eqs. (4)–(8). Critical value α_c is a function of the ratio N_2/N_1.

Using the normalization condition $\int |\psi_i'(r')|^2 d^3r' = 1$, one can determine the chemical potentials μ_i' as functions of N_1, N_2, and α. Analytic expressions for μ_i' are different for $\alpha < \alpha_c$ and for $\alpha > \alpha_c$. In the former case, one has

$$\frac{(\mu_1')^{(5/2)}}{(\mu_1^0)^{(5/2)}} = \frac{1}{1 - \frac{5}{2}R^3[1 - \gamma^2] + \frac{3}{2}R^5}, \qquad (12)$$

$$\frac{(\mu_1')^{(5/2)}}{(\mu_2^0)^{(5/2)}} = \frac{2}{5}\left[\frac{R^3}{3}\left[\frac{\mu_2'}{\mu_1'} - \tilde{\kappa}^2\right] - \frac{R^5}{5}\right]^{-1}, \qquad (13)$$

where $\mu_0' = (15\lambda u_i/8\pi)^{2/5}$, $\gamma = 2\alpha\kappa/(\kappa - 1)$, $\tilde{\kappa} = \gamma/\kappa$. In the limit $\alpha \longrightarrow 0$, one has the results obtained in our previous papers for the nondisplaced potential [10, 11]. In the case $\alpha > \alpha_c$, the formulas for μ_1' and μ_2' obtained after tedious but straightforward calculations are rather cumbersome and will be given elsewhere. In this article, we discuss the results of calculations. To be specific, we will use the parameters corresponding to the experiments on ^{87}Rb atoms: $a_\perp = 2.4 \times 10^{-4}$ cm, $N = N_1 + N_2 = 5 \times 10^6$ atoms, $\lambda = \sqrt{8}$.

In Fig. 1, we show the density profiles of the condensates [see Eqs. (4) and (5)] as functions of the vertical coordinate z for $r'^2 = 0$ and $N_1 = N_2$. In this case, $\alpha_c = 0.0047$. Figure 1a illustrates the experimental situation [7]: $\alpha = 0.03$ (approximately 3% of the extent of the density distribution in the vertical direction) is larger than the critical value α_c, and condensates are completely separated in the vertical direction, in accordance with the experiment [7]. In the case $\alpha < \alpha_c$, the condensate N_2 is inside the condensate N_1. It should be noted that rather small shifts of the trapping potential centers with respect to each other produce considerable displacements of the condensates. The condensates in Fig. 1 do not overlap, because, as was mentioned earlier, in the framework of TFA it is impossible to describe the overlap of the condensates.
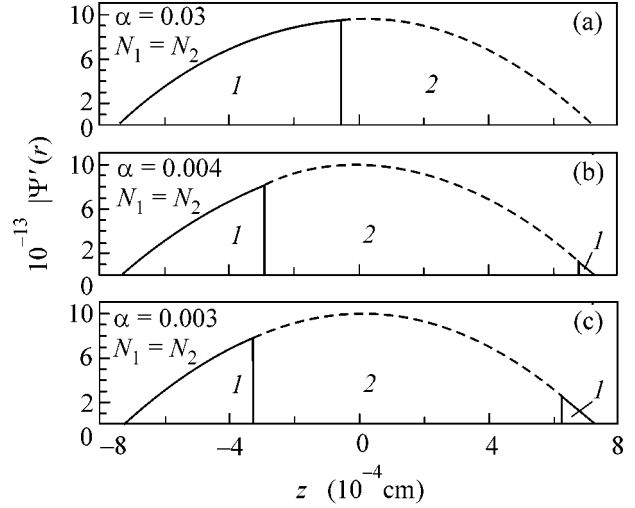
Fig. 1. Density profiles of the condensates as functions of the vertical coordinate z for $N_1 = N_2$. Panel (a) corresponds to $\alpha > \alpha_c$ and panels (b) and (c) to $\alpha < \alpha_c$. Solid lines correspond to the $|1\rangle$ atoms and dashed lines to the $|2\rangle$ atoms.

Another interesting question is how the vortex states change when the minima of the trapping potentials V_1 and V_2 are displaced with respect to each other. In a frame rotating with the angular velocity Ω along the z axis, the energy functional of the system is

$$E_{rot}(l_1, l_2) = E(\psi_{l_1}, \psi_{l_2}) \\ + \int d^3r(\psi_{l_1}^* + \psi_{l_2}^*)i\hbar\Omega\partial_\phi(\psi_{l_1} + \psi_{l_2}), \qquad (14)$$

where $\psi_{l_j}(\mathbf{r}) = |\psi_{l_j}(\mathbf{r})|e^{il_j\phi}$ is the wave function for the vortex excitation with angular momentum $\hbar l_j$. In the TFA, the vortex-induced change in condensate density is negligible [20] (hydrodynamic approximation).

In the case of the phase-segregated condensate, one finds from Eqs. (14) and (6)–(7) that the energy change due to the presence of the vortices $\Delta E = E_{rot}(l_1, l_2) - E_{rot}(0, 0)$ has the following form [10, 11]:

$$\Delta E = \Delta E_{N_1} + E_{N_2}$$

$$= \frac{1}{2}\hbar\omega N_1\int d^3r'\left(\frac{l_1^2}{\rho'^2}|\psi_1'|^2 - \frac{2\Omega l_1}{\omega}|\psi_1'|^2\right) \qquad (15)$$

$$+ \frac{1}{2}\hbar\omega N_2\int d^3r'\left(\frac{l_2^2}{\rho'^2}|\psi_2'|^2 - \frac{2\Omega l_2}{\omega}|\psi_2'|^2\right).$$

In the hydrodynamic limit, ψ_i' is given by Eqs. (4) and (5).

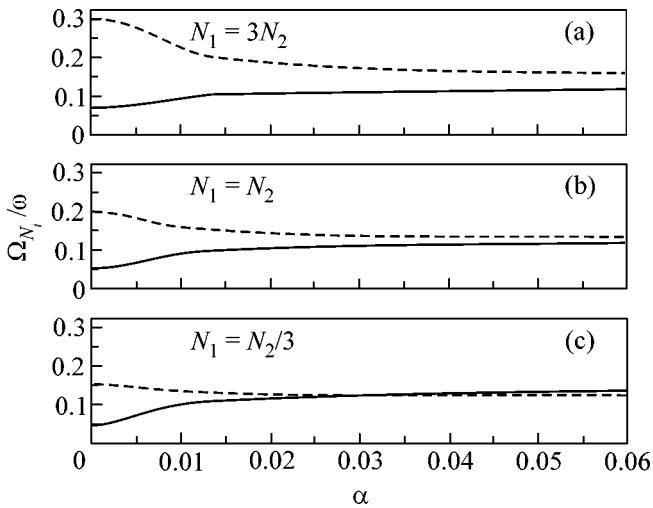**Fig. 2.** Critical velocities of the outer condensate Ω_{N_1}/ω and the inner condensate Ω_{N_2}/ω as functions of α for different values of N_2/N_1. Dashed lines correspond to Ω_{N_2}/ω and solid lines to Ω_{N_1}/ω.

In the case $\alpha = 0$, critical velocities as functions of ratio N_2/N_1 were calculated in [10]. It was shown that, for all values of N_2/N_1, the critical velocity Ω_{N_2} of the inner condensate is lower than the critical velocity Ω_{N_1} of the outer one. So, upon increasing Ω, a vortex will appear first in the external condensate. However, if for a given Ω one shifts the centers of the trapping potentials with respect to each other in the vertical direction, the inner condensate floats to the surface. In this case, one can expect that the critical velocities of the condensates become closer and can even be equal for some values of Ω and N_2/N_1.

As in the case of the chemical potentials, the expressions for the critical velocities have different analytic forms for $\alpha < \alpha_c$ and for $\alpha > \alpha_c$, the latter being rather cumbersome. For $\alpha < \alpha_c$, the critical velocities are given by

$$\frac{\Omega_{N_1}}{\omega} = \frac{5l_1(\mu_1')^{(3/2)}}{2(\mu_1^0)^{(5/2)}}\left\{\left(\ln\frac{2\mu_1'}{l_1} - \frac{4}{3}\right)\right.$$

$$\left. - \frac{3}{2}R\left[\left(1-\gamma^2-\frac{R^2}{3}\right)\ln\frac{2R\mu_1'}{l_1} - \left(1-\gamma^2-\frac{R^2}{9}\right)\right]\right\}, \quad (16)$$

$$\frac{\Omega_{N_2}}{\omega} = \frac{15l_2(\mu_1')^{(3/2)}R}{4(\mu_2^0)^{(5/2)}}\left[\left(\frac{\mu_2'}{\mu_1'} - \tilde{\kappa}^2 - \frac{R^2}{3}\right)\right.$$

$$\left. \times \ln\frac{2R\sqrt{\mu_1'\mu_2'}}{l_2} - \left(\frac{\mu_2'}{\mu_1'} - \tilde{\kappa}^2 - \frac{R^2}{9}\right)\right]. \quad (17)$$

Again, in the limit $\alpha \longrightarrow 0$ one has the results obtained in our previous paper for the nondisplaced potential [10].

Figure 2 shows the behavior of critical velocities as functions of α for different values of N_2/N_1. Dashed lines correspond to the inner condensate and solid lines, to the outer one. From Fig. 2c, one can see that the critical velocities really can intersect. Physically, this means that there is a possibility of exchanging the vortex states between condensates by shifting the centers of the trapping potentials with respect to each other at fixed angular velocities.

In summary, we have investigated the behavior of simultaneously trapped condensates consisting of ^{87}Rb atoms in two different hyperfine states. It is shown that the small shift of the minima of the trapping potentials with respect to each other leads to the considerable displacement of the centers of mass of the condensates, in agreement with the experiment [7]. It is also shown that the critical angular velocities of the vortex states of the condensates strongly depend on the shift and relative number of particles in the condensates. The predicted exchange of the vortex states between the condensates as a function of the shift remains to be studied experimentally.

REFERENCES

1. M. N. Anderson, J. R. Ensher, M. R. Matthews, *et al.*, Science **269**, 198 (1995).

2. K. B. Davis, M.-O. Mewes, M. R. Anderews, *et al.*, Phys. Rev. Lett. **75**, 3969 (1995).

3. C. C. Bradley, C. A. Sackett, and R. G. Hulet, Phys. Rev. Lett. **78**, 985 (1997).

4. K. W. Madison, F. Chevy, W. Wohlleben, *et al.*, Phys. Rev. Lett. **84**, 806 (2000).

5. M. R. Matthews, B. P. Anderson, P. C. Haljan, *et al.*, Phys. Rev. Lett. **83**, 2498 (1999).

6. J. E. Williams and M. J. Holland, Nature **401**, 568 (1999).

7. D. S. Hall, M. R. Matthews, J. R. Ensher, *et al.*, Phys. Rev. Lett. **81**, 1539 (1998).

8. M. R. Matthews, D. S. Hall, D. S. Jin, *et al.*, Phys. Rev. Lett. **81**, 243 (1998).

9. D. S. Hall, M. R. Matthews, C. E. Wieman, *et al.*, Phys. Rev. Lett. **81**, 1543 (1998).

10. S. T. Chui, V. N. Ryzhov, and E. E. Tareyeva, Zh. Éksp. Teor. Fiz. **118**, 1366 (2000) [JETP **91**, 1183 (2000)].

11. S. T. Chui, V. N. Ryzhov, and E. E. Tareyeva, Phys. Rev. A **63**, 023605 (2001).

12. L. P. Pitaevskiĭ, Zh. Éksp. Teor. Fiz. **40**, 646 (1961) [Sov. Phys. JETP **13**, 451 (1961)]; E. P. Gross, Nuovo Cimento **20**, 454 (1961); J. Math. Phys. **4**, 195 (1963).

13. G. Baym and C. J. Pethick, Phys. Rev. Lett. **76**, 6 (1996).

14. F. Dalfovo and S. Stringari, Phys. Rev. A **53**, 2477 (1996).

15. L. D. Landau and E. M. Lifshitz, *Course of Theoretical Physics*, Vol. 5: *Statistical Physics* (Nauka, Moscow, 1976; Pergamon, Oxford, 1980), Part 1.

16. L. P. Pitaevskiĭ, Usp. Fiz. Nauk **168**, 641 (1998) [Phys. Usp. **41**, 569 (1998)].

17. P. Ohberg and S. Stenholm, Phys. Rev. A **57**, 1272 (1998).

18. S. T. Chui and P. Ao, Phys. Rev. A **59**, 1473 (1999).

19. P. Ao and S. T. Chui, Phys. Rev. A **58**, 4836 (1998).

20. A. L. Fetter, cond-mat/9811366; in *Bose–Einstein Condensation in Atomic Gases Proceedings of the International School of Physics "Enrico Fermi," Varenna, 1998*, Ed. by M. Inguscio, S. Stringari, and C. E. Wieman (IOS Press, Amsterdam, 1999).

Superconducting Energy Gap Distribution in *c*-Axis Oriented MgB$_2$ Thin Film from Point Contact Study[1]

Yu. G. Naidyuk[1, *], I. K. Yanson[1], L. V. Tyutrina[1], N. L. Bobrov[1], P. N. Chubov[1], W. N. Kang[2], Hyeong-Jin Kim[2], Eun-Mi Choi[2], and Sung-Ik Lee[2]

[1] Verkin Institute for Low Temperature Physics and Engineering, National Academy of Sciences of Ukraine, Kharkiv, 61103 Ukraine
* e-mail: naidyuk@ilt.kharkov.ua
[2] National Creative Research Initiative Center for Superconductivity, Department of Physics, Pohang University of Science and Technology, 790-784 Pohang, South Korea
Received January 17, 2002

We have analyzed about a hundred voltage-dependent differential resistance $dV/dI(V)$ curves of metallic point contacts between *c*-axis-oriented MgB$_2$ thin film and Ag, which exhibit clear Andreev reflection features connected with the superconducting gap. About one half of the curves show the presence of a second larger gap. The histogram of the double gap distribution reveals distinct maxima at 2.4 and 7 meV, while curves with single-gap features result in a more broad maximum at 3.5 meV. The double-gap distribution is in qualitative agreement with the distribution of gap values over the Fermi surface calculated by H.J. Choi *et al.* (cond-mat/0111183). The data unequivocally show the presence of two gaps: $\Delta_S = 2.45 \pm 0.15$ meV and $\Delta_L = 7.0 \pm 0.45$ meV in MgB$_2$ with the gap ratio $\Delta_L/\Delta_S = 2.85 \pm 0.15$. Our observations further prove a widely discussed multigap scenario for MgB$_2$, where two distinct gaps are seen in the clean limit, while a single averaged gap is present in the dirty one. © *2002 MAIK "Nauka/Interperiodica"*.

PACS numbers: 73.40.Jn; 74.76.Db; 74.80.Fp

INTRODUCTION

Direct spectroscopic investigations of the superconducting order parameter in the recently discovered [1] superconductor MgB$_2$ with $T_c \simeq 40$ K by tunneling [2–10] and point-contact spectroscopy [10–17] unambiguously show an energy gap Δ in the quasiparticle density of states (DOS). However, the experimental results are controversial with respect to the gap width Δ, whose variation from 1.5 to 8 meV (see, e.g., review [18]) is unexpectedly large, pointing to the possibility of multiphase or nonhomogeneous samples, a degraded surface, or an anisotropic energy gap. Another way to solve this puzzle is to consider two superconducting gaps in MgB$_2$, as proposed by Liu *et al.* [19], accounting for the complex electronic structure of MgB$_2$ with both a quasi-2D and 3D Fermi surface [20]. Indeed, several papers [6–8, 15–17] have reported a double-gap structure in the differential conductance (resistance), with the smaller gap being far below the weak-coupling BCS value $\Delta = 1.76 k_B T_c \simeq 6$ meV and the larger gap slightly above the standard BCS one, in accordance with theory [19].

Therefore, one of the intriguing key issues of the superconducting state of MgB$_2$ is whether the double gap state is intrinsic or the spread of the gap values is a result of anisotropy, nonhomogeneity, surface effect, etc. In other words, before high-quality macroscopic single crystals will be available for thorough investigations, the sample imperfection may raise doubts about the final conclusion. However, in our opinion, good reproducibility of the double-gap values given by different authors [6–8, 15–17] by different, in their physical background, methods, such as tunneling and point-contact spectroscopy, carried out on different samples such as pellets, films, and grains (all this with a great degree of probability) supports the intrinsic nature of the double gap in MgB$_2$.

In this paper, we will give further confirmation of the double-gap scenario in MgB$_2$ based on an analysis of about a hundred point-contact spectra of *c*-axis-oriented thin films.

EXPERIMENTAL AND CALCULATION DETAILS

We measured a high-quality *c*-axis-oriented 0.4-μm thick MgB$_2$ film [21] grown by the PLD technique on Al$_2$O$_3$ substrate. The resistivity of the film exhibits a sharp transition at 39 K with a width of ~0.2 K from 90% to 10% of the normal-state resistivity [21]. The residual resistivity ρ_0 at 40 K is ~6 μΩ cm[2] and *RRR* = 2.3.

---

[1] This article was submitted by the authors in English.

[2] There is a scattering by a factor of 4 in ρ_0 for different films.

Different point contacts (PCs) were established *in situ* directly in liquid ^{4}He by touching the as-prepared surface (sometimes etched by 1% HCl solution in ethanol) of the MgB_2 film by the sharpened edge of an Ag counter electrode, which was cleaned by chemical polishing in HNO_3. This geometry corresponds to the current flowing preferably along the *c* axis. A number of contacts were measured by touching the film edge after breaking the Al_2O_3 substrate. In this way, the current flows preferably along the *ab* plane. The differential resistance *dV/dI* vs. *V* was recorded using a standard lock-in technique. The normal resistance R_N (at $V \gg \Delta$) of the investigated contacts ranged mainly between 10 and 1000 Ω at 4.2 K.

The important characteristic of PC is their size or diameter *d*, which can be determined from the simple formula derived by Wexler [22] for contact resistance:

$$R_{PC}(T) \simeq \frac{16\rho l}{3\pi d^2} + \frac{\rho(T)}{d}, \qquad (1)$$

where the two terms represent ballistic Sharvin[3] and diffusive Maxwell resistance, correspondingly. Here $\rho l = p_F/ne^2$, where p_F is the Fermi momentum and *n* is the density of charge carriers. The latter for MgB_2 is estimated at $n \simeq 6.7 \times 10^{22}$ [23], which results in $\rho l \simeq 2 \times 10^{-12}$ Ω cm^2 using $v_F \simeq 5 \times 10^7$ cm/s [20]. Hence, the upper limit for the elastic mean free path $l = \rho l/\rho_0$ for our film is about 3 nm. In this case, according to Eq. (1), the condition $d < l$ is fulfilled for PC with $R > 40$ Ω or for a lower resistance, supposing multiple contacts in parallel.

We used the conventional Blonder–Tinkham–Klapwijk equations [24] describing the *I–V* characteristic of ballistic N–c–S metallic junctions (here N is the normal metal, c is the constriction, and S is the superconductor) by accounting for the processes of the Andreev reflection. At finite barrier strength at the N–S interface characterized by parameter $Z \neq 0$ and $T \ll T_c$, the theory gives *dV/dI* curves with minima at $V \simeq \pm\Delta/e$. To get the correct Δ, the measured curves should be fitted to the theory. The additional smearing of *dV/dI* curves due to, e.g., broadening of the quasiparticle DOS in the superconductor, can be taken into account by including parameter Γ [25].

In the case of curves with a double-gap structure, we calculated, according to the theory [24], the sum of two differential conductances *dI/dV* with the weight *w* for the larger gap and, correspondingly, with $(1 - w)$ for the smaller one. After this, we transformed *dI/dV* into *dV/dI* to compare with the measured dependences. The best fit was achieved, as a rule, by using its own values of *Z* and Γ for the large and small gaps. It is acceptable if we suppose that we have a number of microconstrictions with various *Z* in the region of mechanical contact. It is note

---

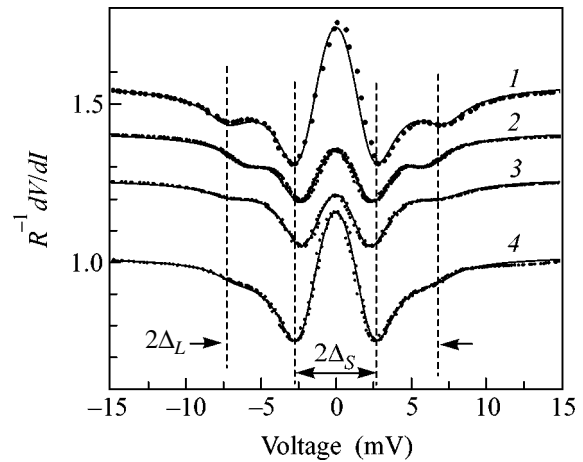[3] In the case of interface scattering, Sharvin resistance should be multiplied by the factor $(1 + Z^2)$ [24].

Fig. 1. Reduced differential resistance R_N^{-1} *dV/dI* vs. *V* measured at $T = 4.2$ K for four MgB_2–Ag contacts with a double-gap structure (symbols). Thin lines are theoretical dependences calculated with parameters given in Table 1. The curves (*1–3*) are vertically offset for clarity. Vertical dashed lines show approximate positions of large Δ_L and small Δ_S gaps. Experimental curves are taken nominally in *c* directions.

worthy that, with increasing weight factor, the difference between the *Z* and Γ values for large and small gaps becomes smaller or even vanishes for some PCs.

RESULTS AND DISCUSSION

Approximately one half (44 of total 91) of the analyzed raw *dV/dI* vs. *V* curves show a visible two-gap structure, although, in most cases, with shallow features corresponding to a larger gap. The samples of some *dV/dI* curves taken at 4.2 K $\ll T_c$ with the double-gap structure, along with calculated curves, are shown in Fig. 1. In spite of a number of fitting parameters (Δ, Γ, *Z*, ω) for curves with pronounced (or at least visible as shown in Fig. 1) double-gap features, the determined, the Δ_L and Δ_S are robust with respect to the fitting procedure.

Table 1. Fitting parameters for curves presented in Fig. 1

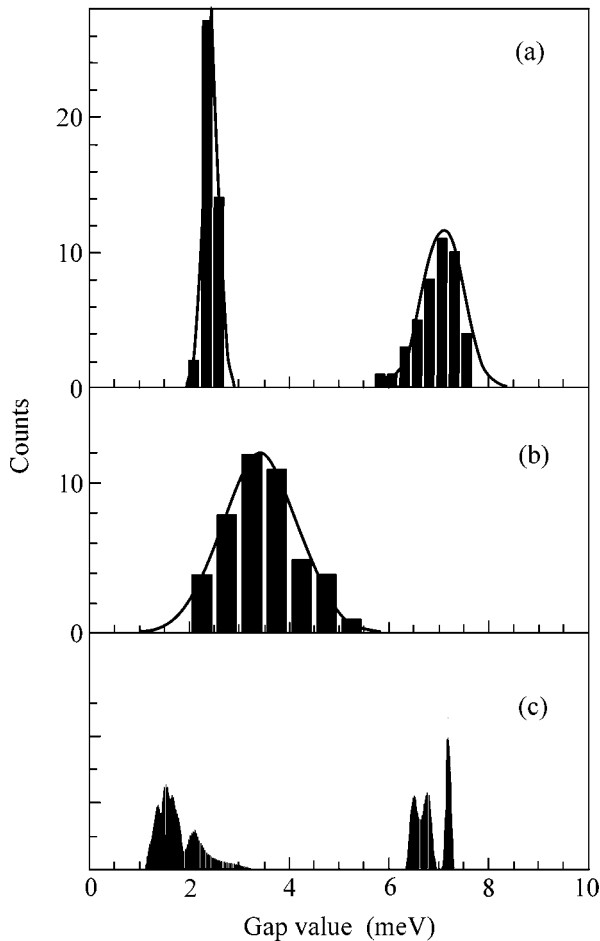| Parameters	Curve *1*	Curve *2*	Curve *3*	Curve *4*
R_N, Ω	47	35	20	34
Δ_L, meV	7.4	6.25	7.35	7.3
Δ_S, meV	2.6	2.54	2.4	2.6
w-factor	0.11	0.08	0.07	0.06
Z_L	0.7	0.71	0.63	0.21
Z_S	0.75	0.55	0.56	0.76
Γ_L, meV	0.4	0.1	0.55	0
Γ_S, meV	0.5	0.54	0.38	0.3

Fig. 2. The superconducting energy-gap distribution in *c*-axis-oriented MgB$_2$ thin film in the case: (a) double gap and (b) single gap. Thin lines show Gaussian fit with maxima at (a) 2.45 and 7 meV and (b) 3.5 meV. The histogram window of 0.25 meV for (a) and 0.5 meV for (b) is chosen to achieve the most close to normal (Gaussian) distribution. (c) Distribution of gap values over the Fermi surface calculated in [26].
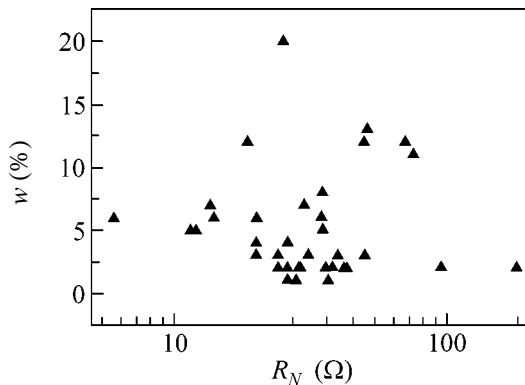

Fig. 3. Dependence of the weight factor *w* on the point-contact resistance.

It turns out that the histogram of the distribution of gaps built on the basis of fitting 44 spectra (see Fig. 2a) has two well-separated and quite narrow (especially for the small gap) maxima.

The double-gap distribution is in qualitative agreement with the distribution of gap values over the Fermi surface, which was recently calculated in [26] (see Fig. 2c). The main difference is that the theoretical distribution for the lower gap is wider and has a dominant maxima around 1.6 meV. This discrepancy can be resolved if we consider that we have measured curves with a double-gap structure for contacts that are predominantly along the *c* axis. In this case, according to [26], the gap values along the *c* axis spread between 2 and 3 meV. The *c*-axis directionality of our measurements is, apparently, the main reason for a shallow large-gap structure in *dV/dI*, because the large gap dominates in the "a–b" plane [26].

It should be mentioned that two very different order parameters exist only in the clean limit $l \gg 2\pi\xi$. Since in our case *l* has an upper limit at 3 nm and the coherence length $\xi \sim 5$ nm [27], the observation of two gaps is in line with our supposition that in the PC area there are small grains with a much larger mean free path. Indeed, the SEM image of MgB$_2$ films [16] shows that the film is granular with 100- to 500-nm grains. Therefore, in the area of mechanical contact there is some amount of small metallic bridges, perhaps, with a slightly different crystallographic orientation being in parallel.

The single gap Δ is seen for the dirty limit[4] and is the average of small and large gaps with some weights. If we assume that this weight has some relation to the weight *w* used in the fitting procedure, then, admittedly, $\Delta \simeq w\Delta_L + (1 - w)\Delta_S = 3.4$ meV by using the upper limit $w \simeq 0.2$ (see Fig. 3). This agrees with the position of the maximum of the single-gap distribution at 3.5 meV (see Fig. 2b). In addition, according to the calculation in [28], a large amount of impurity scattering will cause the gaps to converge to $\Delta \simeq 4.1$ meV.

Therefore, the superconducting properties of this compound can be strongly influenced by nonmagnetic defects and impurities, which seem to have a great impact also on the scattering of gap value(s) given by different authors.

As to the *w* factor, it is hardly to see in Fig. 3 its dependence on R_N or PC size, which one would expect if the small gap reflects a degraded surface or the large gap is a result of surface states [29].

Table 2 shows double-gap values given by different authors. Good correspondence between our results and data of other authors carried out on different types of MgB$_2$ samples is evident. In our case of averaging over

---

[4] On *dV/dI* of "edge" contacts (a total of 11 curves) only single-gap structure was observed, probably due to the deterioration of the film edge after breaking.

Table 2. Gap values in MgB_2 measured by point-contact (PCs) or tunneling spectroscopy (TS)

Method	Sample	Δ_S, meV	Δ_L, meV	Ref.
PCs	Film	2.45 ± 0.15	7.0 ± 0.4	This pap.
PCs	Film	2.3 ± 0.3	6.2 ± 0.7	[16]
PCs	Grain	2.8	7	[15]
TS	Granular	3.9	7.5	[6]
TS	50μ crys.	3.8	7.8	[7]
TS	polycrys	1.75	8.2	[8]

44 curves, the ratio of the larger gap to the lower one of 2.85 ± 0.15 is close to the theoretical value of 3 : 1 [19].

CONCLUSION

We have analyzed dV/dI point-contact spectra of MgB_2 with clear single- and double-gap structures. The observed distinct maxima in the double-gap distribution, which is consistent with the theoretical calculations [26], ruled out the surface or multiphase origin of the gap structure and testify to the intrinsic superconducting double-gap state in MgB_2. The averaged gap value ratio turned out to be in accordance with the theoretically predicted ratio 1 : 3 [19].

REFERENCES

1. J. Nagamatsu, N. Nakagawa, T. Muranaka, *et al.*, Nature **410**, 63 (2001).
2. G. Karapetrov, M. Javarone, W. K. Kwok, *et al.*, Phys. Rev. Lett. **86**, 4374 (2001).
3. G. Rubio-Bollinger, H. Suderow, and S. Vieira, Phys. Rev. Lett. **86**, 5582 (2001).
4. A. Sharoni, I. Felner, and D. Millo, Phys. Rev. B **63**, 220508(R) (2001).
5. P. Seneor, C.-T. Chen, N.-C. Yeh, *et al.*, Phys. Rev. B **65**, 012505 (2002).
6. F. Giubileo, D. Roditchev, W. Sachs, *et al.*, cond-mat/0105146.
7. F. Giubileo, D. Roditchev, W. Sachs, *et al.*, Phys. Rev. Lett. **87**, 177008 (2001).
8. M. H. Badr, M. Freamat, Y. Sushko, and K.-W. Ng, cond-mat/0110421.
9. Y. Zhang, D. Kinion, J. Chen, *et al.*, cond-mat/0107478.
10. H. Schmidt, J. F. Zasadzinski, K. E. Gray, *et al.*, Phys. Rev. B **63**, 220504R (2001).
11. A. Kohen and G. Deutscher, Phys. Rev. B **64**, 060506(R) (2001).
12. A. Plecenik, Š. Beňačka, P. Kúš, *et al.*, Physica C **368**, 251 (2002).
13. F. Laube, G. Goll, J. Hagel, *et al.*, Europhys. Lett. **56**, 296 (2001).
14. R. S. Gonnelli, A. Calzolari, D. Daghero, *et al.*, cond-mat/0107239.
15. P. Szabó, P. Samuely, J. Kacmarćik, *et al.*, Phys. Rev. Lett. **87**, 137005 (2001).
16. Y. Bugoslavsky, Y. Miyoshi, G. K. Perkins, *et al.*, cond-mat/0110296.
17. N. L. Bobrov, P. N. Chubov, Yu. G. Naidyuk, *et al.*, cond-mat/0110006.
18. C. Buzea and T. Yamashita, Supercond. Sci. Technol. **14** (11), R115 (2001).
19. A. Y. Liu, I. I. Mazin, and J. Kortus, Phys. Rev. Lett. **87**, 087005 (2001).
20. J. Kortus, I. I. Mazin, K. D. Belashchenko, *et al.*, Phys. Rev. Lett. **86**, 4656 (2001).
21. W. N. Kang, Hyeong-Jin Kim, Eun-Mi Choi, *et al.*, Phys. Rev. Lett. **87**, 087002 (2001).
22. A. Wexler, Proc. Phys. Soc., London **89**, 927 (1966).
23. P. C. Canfield, D. K. Finnemore, S. L. Bud'ko, *et al.*, Phys. Rev. Lett. **86**, 2423 (2001).
24. G. E. Blonder, M. Tinkham, and T. M. Klapwijk, Phys. Rev. B **25**, 4515 (1982).
25. R. C. Dynes, V. Narayanamurti, and J. P. Garno, Phys. Rev. Lett. **41**, 1509 (1978).
26. Hyoung Joon Choi, David Roundy, Hong Sun, *et al.*, cond-mat/0111183.
27. D. K. Finnemore, J. E. Ostenson, S. L. Bud'ko, *et al.*, Phys. Rev. Lett. **86**, 2420 (2001).
28. A. Brinkman, A. A. Golubov, H. Rogalla, *et al.*, cond-mat/0111115.
29. V. D. P. Servedio, S.-L. Drechsler, and T. Mishonov, cond-mat/0111434.

Dynamic Orientational Phase Transition in a Two-Layer Magnetically Coupled Structure

D. I. Sementsov and A. M. Shutyĭ

Ul'yanovsk State University, ul. L'va Tolstogo 42, Ul'yanovsk, 432700 Russia

Received February 13, 2002

The magnetization dynamics was studied for a system of two magnetic layers separated by a nonmagnetic spacer providing their antiferromagnetic coupling. A new effect of orientational phase transition occurring upon a change in the amplitude (frequency) of a microwave field was observed near the edge of the orientational hysteresis loop. © 2002 MAIK "Nauka/Interperiodica".

PACS numbers: 75.70.Cn; 75.30.Kz

1. The uniqueness and broad spectrum of static and dynamic properties of multilayer structures composed of alternating layers of a ferromagnetic metal and a nonmagnetic material are primarily due to the diversity of coupling types between the layer magnetizations and to the nonlinear character of their interaction with an external field [1–3]. Various types of coupling give rise to various types of equilibrium magnetic ordering driven by an external magnetic field [4, 5]. Of particular interest are the properties of such structures near the critical fields corresponding to the orientational phase transitions accompanied by a jumpwise change in the layer magnetizations. For instance, field domains in which the states of orientational bistability showed up as the orientational hysteresis and jumpwise rearrangement of magnetization were observed in [6] for a system of two antiferromagnetically coupled magnetic films.

The character of magnetic ordering in a multilayer structure largely determines the resonance behavior of its spin subsystem in a high-frequency field [7, 8]. The nonlinear interaction of an alternating field with the magnetic moments of the layers also gives rise to a number of dynamic effects, namely, to an increase in the precession angle [9] and to dynamic bistability and fractionation [10], which occur even in a system of two magnetic moments with dipolar coupling [11, 12]. A search for the conditions under which various dynamic regimes can be excited by a high-frequency field is of interest in many practical applications. In this work, the dynamic magnetization reversal occurring near the edge of an orientational hysteresis loop in the course of precession under the action of a high-frequency field is studied for a two-layer structure with antiferromagnetic coupling.

2. Let us consider a structure composed of two ferromagnetic layers and a nonmagnetic spacer between them. Each of the magnetic layers has thickness d_i, magnetization $\mathbf{M}_i$, and in-plane uniaxial anisotropy with the anisotropy constant K_i. The external magnetic field $\mathbf{H}$ is aligned with the easy axis common to both layers, and the high-frequency field $\mathbf{h}(t)$ is linearly polarized in the film plane and is perpendicular to the external magnetic field. In this case, the energy of a magnetic subsystem per a film unit area is

$$
\begin{aligned}
E = \sum_{i=1,2} d_i \{ &K_i \sin^2 \varphi_i - HM_i \cos \varphi_i \\
&- hM_i \sin \varphi_i \cos \psi_i - 2\pi M_i^2 \cos^2 \psi_i \} \\
+ AM_1 M_2 d_{12} [&\cos \psi_1 \cos \psi_2 \cos(\varphi_1 - \varphi_2) \\
&+ \sin \psi_1 \sin \psi_2],
\end{aligned}
\tag{1}
$$

where $d_{12} = d_1 d_2 (d_1 + d_2)^{-1}$ is the reduced thickness of the two magnetic layers; A is their coupling constant depending, in the general case, on the spacer thickness, material, and its structural characteristics; the azimuthal angle φ_i measured from the y axis, and the angle ψ_i of departure from the film plane specify the directions of vector $\mathbf{M}_i$ in the horizontal and vertical planes.

The equations of motion for the magnetization vectors $\mathbf{M}_i$ of each layer are written as

$$
\begin{aligned}
\dot{\varphi}_i M_i d_i \sin \psi_i &= \gamma \frac{\partial E}{\partial \psi_i} + \frac{\lambda_i}{M_i} \frac{1}{\sin \psi_i} \frac{\partial E}{\partial \varphi_i}, \\
\dot{\psi}_i M_i d_i &= \frac{\lambda_i}{M_i} \frac{\partial E}{\partial \psi_i} - \gamma \frac{1}{\sin \psi_i} \frac{\partial E}{\partial \varphi_i},
\end{aligned}
\tag{2}
$$

where γ is the gyromagnetic ratio and λ_i are the damping parameters in the respective layers [13]. The linear approximation in small deviations from equilibrium position ($\delta_i = \varphi_i - \varphi_{0i}$ and ψ_i) yields the following

expression for the susceptibility of the system and its layers [14]:

$$\chi = (d_1\chi_1 + d_2\chi_2)(d_1 + d_2)^{-1},$$

$$\chi_i = 4\pi\gamma^2 M_i \frac{M_i\Delta_{3-i}\cos\varphi_{0i} - 4\pi\gamma^2 D_i M_{3-i}\cos\varphi_{03-i}}{\Delta_1\Delta_2 - 16\pi^2\gamma^4 D_1 D_2}. \quad (3)$$

Here, the quantities $\Delta_i = \omega_{0i}^2 - \omega^2 - 4\pi\gamma^2 D_i + 4\pi i\lambda_i\omega$, where

$$D_i = Ad_{12}M_1M_2\cos(\varphi_{0i} - \varphi_{03-i})/d_i,$$

$$\omega_{0i}^2 = 4\pi M_i\gamma^2[H\cos\varphi_{0i} + H_{ki}\cos 2\varphi_{0i}]$$

are the resonance frequencies of the isolated layers and $H_{ki} = 2K_i/M_i$ is the magnetic anisotropy field of the ith layer.

3. A two-layer magnetically coupled structure with a nonmagnetic spacer and the antiferromagnetic type of interaction between the magnetic moments of the layers ($A > 0$) may undergo orientational phase transitions resulting in collinear and noncollinear states of the film magnetic moments [6]. If the system has the states with two or three stationary orientations of magnetic moments (at $H = $ const), then variously shaped orientational hysteresis loops can appear upon changing the magnetic field. Near the edges of the hysteresis loop, the system is expected to be most sensitive to the microwave field. We will study the dynamic behavior of the system near the critical field H_c, where the state with oppositely directed film magnetic moments ceases to be stable. In the calculations, we will use parameters close to the parameters of real films of the Permalloy class: $\lambda_1 = \lambda_2 = 5 \times 10^7$ s^{-1}; anisotropy field and magnetization of the first film $H_{k1} = 10$ Oe and $4\pi M_1 = 1.1 \times 10^4$ G, respectively, and $H_{k2} = 5$ Oe and $4\pi M_2 = 8 \times 10^3$ G for the second film; $\gamma = 1.76 \times 10^7$ Oe^{-1} s^{-1}; and the thicknesses of both films are chosen to be equal; i.e., $d_1 = d_2 = 0.1$ μm.

Numerical analysis of the equations of motion (2) shows that, if the magnetic field is close to its critical value H_c ($H_c - H \leq 0.5$ Oe), then one can choose the microwave amplitude h_c for any frequency ω in such a way that the precession axes are directed oppositely at $h < h_c$, whereas at $h > h_c$ the system undergoes dynamic magnetization reversal from the initial configuration with angles $\varphi_{01} = 0$ and $\varphi_{02} = \pi$ to the state with the codirected precession axes in both films. The transients of azimuthal angles and the steady-state orbits of magnetic moments of the (a) first and (b) second films are shown in Fig. 1 for the coupling constant $A = 0.01$, frequency $\omega = 7 \times 10^9$ s^{-1}, which is close to the resonance frequency ω_{01} of the first film, and microwave amplitudes $h = 0.70$ and 0.71 Oe (curves 1 and 2), which are lower and higher, respectively, than the critical value h_c. The magnetic field $H = 8.6$ Oe is chosen so that for the given coupling constant A it is close to the critical field,
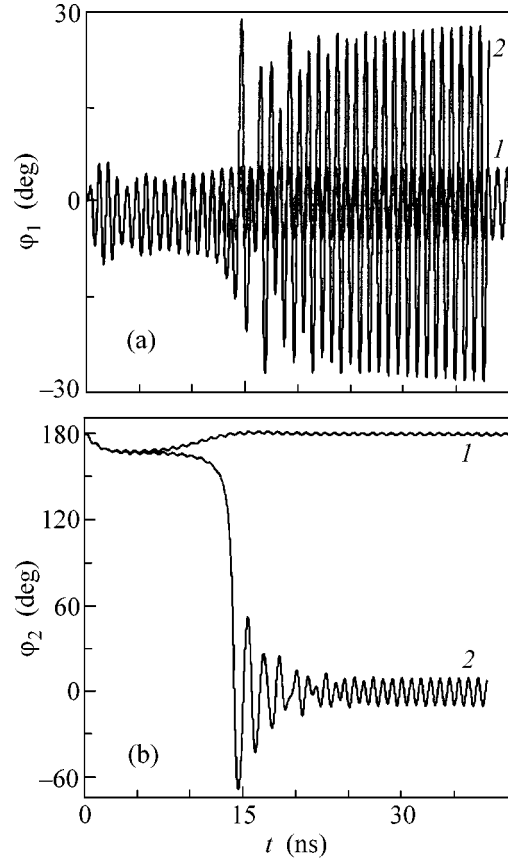

Fig. 1. Time-dependent azimuthal angles of magnetic moments of the first and the second films at frequency $\omega \approx \omega_{01}$ for two microwave amplitudes close to the critical value h_c.

while the directions of the film magnetic moments in the equilibrium state are opposite with angles $\varphi_1 = 0$ and $\varphi_2 = \pi$ in the absence of a microwave field. One can see that the initial stage of establishing precession is virtually the same in both cases. However, small distinctions in the trajectories at this stage lead to the catastrophic changes in the dynamics of magnetic moments of the system, so that the steady-state precession regimes are different. After the dynamic magnetization reversal, the precession amplitude proves to be several times larger, despite the fact that the microwave amplitude increases only slightly. Similar situation can also be obtained when the microwave frequency ω changes in the vicinity of the critical field at a fixed amplitude h.

The frequency-dependent (a) amplitudes $\phi_i = \tilde{\varphi}_i - \varphi_{0i}$ of precession angles in the first and the second films and (b) high-frequency susceptibility $\tilde{\chi} = (M_1\cos\tilde{\varphi}_1 + M_2\cos\tilde{\varphi}_2)/h$, where $\tilde{\varphi}_i$ are the amplitudes of azimuthal angles of steady-state oscillations of the corresponding magnetic moments, are shown in Fig. 2 for the chosen coupling constant and magnetic field and for different
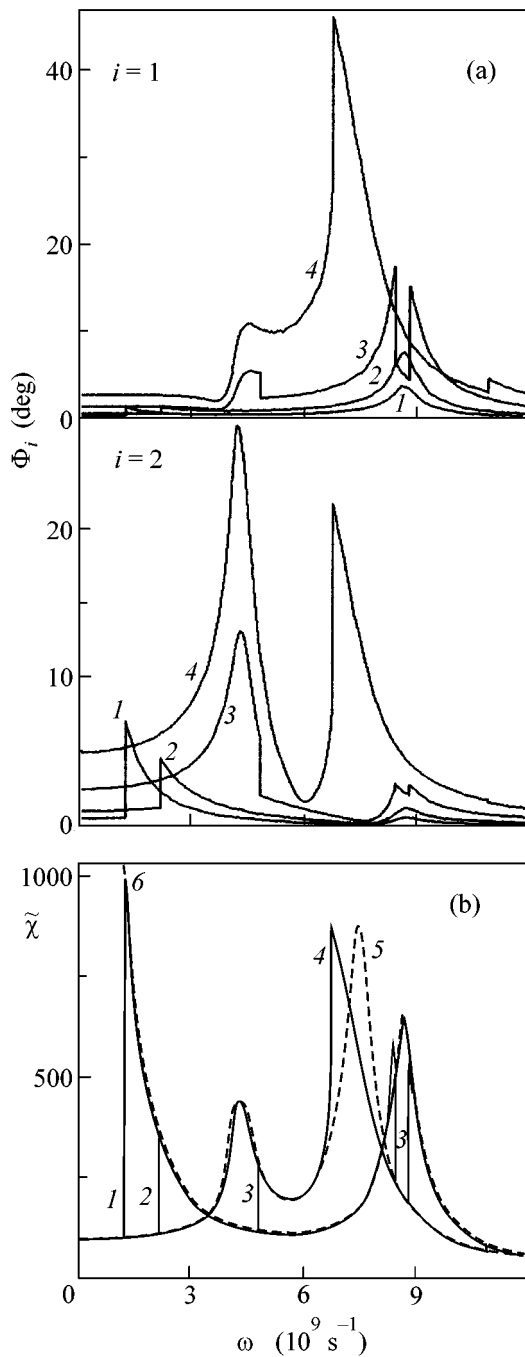
Fig. 2. Frequency-dependent (a) precession angles ϕ_i of magnetic moments of the first and the second films and (b) high-frequency susceptibility $\tilde{\chi}$ of the system for different microwave amplitudes; dashed curves *5* and *6* are the linearized solutions corresponding to $\varphi_{01} = \varphi_{02} = 0$ and $\varphi_{01} = 0$, $\varphi_{02} = \pi$, respectively.

field amplitudes $h = 0.1$, 0.2, 0.5, and 1 Oe (curves *1–4*). The dashed lines in Fig. 2b correspond to the linearized solutions obtained for the equilibrium orientations (curve *5*) $\varphi_{01} = \varphi_{02} = 0$ and (curve *6*) $\varphi_{01} = 0$, $\varphi_{02} = \pi$ using Eq. (3). One can see from these curves that at fre-

quencies $\omega \leq 10^9$ s^{-1} the second film undergoes magnetization reversal even at $h \leq 0.1$ Oe, and both magnetic moments undergo steady-state precession about the codirected axes. Starting at a certain frequency (depending on the microwave amplitude), the magnetization reversal does not occur and the precession axes in the films remain oppositely directed. As the amplitude h increases, the frequency interval of magnetization reversal extends to the larger values. For example, at $h = 0.5$ Oe, it covers only the first resonance region, while, at $h = 1$ Oe, it covers both resonances and the magnetization reversal is absent only at the end of the indicated frequency interval. The presence of a rather narrow magnetization-reversal frequency region contiguous to the resonance frequency of the system in the initial configuration $\varphi_1 = 0$, $\varphi_2 = \pi$ is typical of the effect considered (curve *3*). It is worth noting that a change in the magnetic field H by a few tenths of oersted dramatically alters the intervals of microwave frequencies where the dynamic magnetization reversal occurs.

After the dynamic magnetization reversal, the precession amplitude may both increase compared to the precession about the oppositely directed axes and decrease, depending on the chosen frequency range. Analysis shows that it increases in the frequency interval $\omega_a < \omega < \omega_b$, where the boundary frequencies are found from the equation $|\chi(\varphi_{02} = 0)| = |\chi(\varphi_{02} = \pi)|$. In the structure with equal thicknesses of magnetic layers, the following approximate expressions hold for the cited frequencies if the damping in the spin system is ignored:

$$\omega_a = 2\gamma\sqrt{2\pi K_2},$$
$$\omega_b = \gamma\sqrt{4\pi M_1(H + H_{k1} + M_2 A/2)}. \tag{4}$$

Over a rather broad range of parameters, the frequencies determined by these expressions differ from their true values only by 1–5%.

The analysis carried out in this work indicates that a two-layer magnetically coupled system with antiferromagnetic interaction of the layer magnetic moments undergoes dynamic magnetization reversal under the action of a microwave field. As a result, the oppositely directed magnetic moments in the initial configuration are replaced by the precession about the codirected axes. It is found that a small increase in the amplitude of the microwave field near its critical value may drastically enhance the amplitude of precession caused by the magnetization reversal of one of the layers.

REFERENCES

1. P. Bruno and C. Chappert, Phys. Rev. B **46**, 261 (1992).

2. A. Vedyayev, B. Dieny, N. Ryzhanova, and J. Genin, Phys. Lett. A **158**, 117 (1994).

3. A. Schreyer, J. F. Ankher, Th. Zeidler, *et al.*, Phys. Rev. B **52**, 16066 (1995).

4. V. V. Ustinov, M. M. Kirilova, I. V. Lobov, *et al.*, Zh. Éksp. Teor. Fiz. **96**, 477 (1996) [JETP **82**, 253 (1996)].

5. V. V. Kostyuchenko and A. K. Zvezdin, Phys. Rev. B **57**, 5951 (1998).

6. D. I. Sementsov and A. M. Shutyĭ, Pis'ma Zh. Éksp. Teor. Fiz. **74**, 339 (2001) [JETP Lett. **74**, 306 (2001)].

7. N. G. Bebenin and V. V. Ustinov, Fiz. Met. Metalloved. **84**, 29 (1997).

8. N. M. Kreines, A. N. Kolmogorov, and V. F. Mescheria-kov, J. Magn. Magn. Mater. **1913,** 177 (1998).

9. A. M. Shutyĭ and D. I. Sementsov, Zh. Éksp. Teor. Fiz. **118**, 110 (2000) [JETP **91**, 531 (2000)].

10. S. M. Rezende and F. M. de Aguiar, Proc. IEEE **78** (5), 893 (1990).

11. F. V. Lisovskiĭ and O. P. Polyakov, Pis'ma Zh. Éksp. Teor. Fiz. **68**, 643 (1998) [JETP Lett. **68**, 679 (1998)].

12. F. V. Lisovskiĭ and O. P. Polyakov, Pis'ma Zh. Éksp. Teor. Fiz. **73**, 546 (2001) [JETP Lett. **73**, 483 (2001)].

13. A. G. Gurevich and G. A. Melkov, *Magnetic Oscillations and Waves* (Nauka, Moscow, 1994).

14. D. I. Sementsov and A. M. Shutyĭ, Pis'ma Zh. Tekh. Fiz. **27** (21), 19 (2001) [Tech. Phys. Lett. **27**, 897 (2001)].

Translated by V. Sakun

Anomalous Diffusion and Fluctuation Effects
in Highly Disordered Media

L. A. Bolshov, A. M. Dykhne, and P. S. Kondratenko

Nuclear Safety Institute, Russian Academy of Sciences,
Moscow, 113191 Russia

The model of impurity transport in highly disordered fractal media is generalized with account taken of the superdiffusional behavior at large distances and fluctuative behavior at small distances. It is found that the impurity source power is renormalized due to the spatial fluctuations of medium characteristics. The renormalization coefficient K decreases dramatically with changing the source dimension R for R values smaller than the correlation length in the medium. In the same domain of R values, the coefficient K, together with the effective power, undergoes increasing statistical scatter. © 2002 MAIK "Nauka/Interperiodica".

PACS numbers: 66.30.Jt; 61.43.Hv

The impurity migration in highly disordered media with fractal properties is usually analyzed on the basis of the generalized transport equation, which leads to anomalous diffusion [1, 2]. Such a description has an averaged character. At the same time, it is clear that the local characteristics of a fractal medium strongly fluctuate. The question arises as to how these fluctuations influence the transport processes and how the corresponding effects can be taken into account. In this work, the influence of fluctuations on the impurity transport is analyzed for sources of various size.

The general scheme of the averaged description of impurity transport in a statistically uniform three-dimensional medium can be formulated in terms of the continuity equation

$$\partial c/\partial t + \mathrm{div}\,\mathbf{q} = 0, \tag{1}$$

where the flux density vector $\mathbf{q} = \mathbf{q}(\mathbf{r}, t)$ and the particle concentration $c(\mathbf{r}, t)$ are functions of coordinate and time and related to each other by the relationship

$$q_i(\mathbf{r}, t) = -\int d\mathbf{r}' f_i(\mathbf{r} - \mathbf{r}')\mathbf{c}(\mathbf{r}', \mathbf{t}), \tag{2}$$

and the function $f_i(\mathbf{r})$ is determined by the medium characteristics and has the property

$$\int d\mathbf{r}\, f_i(\mathbf{r}) = 0. \tag{3}$$

If the function $f_i(\mathbf{r})$ decreases at large distances faster than $|\mathbf{r}|^{-4}$, then Eq. (1) reduces to the classical diffusion equation giving the $r(t) \propto t^{1/2}$ law for the migration distance at large times and to the Gaussian law for the concentration decrease at large distances. If the decrease is slower than $|\mathbf{r}|^{-4}$, then, considering that the integral in

Eq. (3) must converge, the asymptotic behavior of the function $f_i(\mathbf{r})$ is expressed by the formula

$$f_i(\mathbf{r})\big|_{|\mathbf{r}| \gg L} \cong d\left(\frac{\mathbf{r}}{|\mathbf{r}|}\right)\frac{V}{L^3}\left(\frac{L}{|\mathbf{r}|}\right)^{4-\alpha}, \quad 0 < \alpha < 1. \tag{4}$$

Here, $d(\mathbf{n}) \sim 1$ for $|\mathbf{n}| = 1$, and V and L are the medium characteristics with dimensions of velocity and length, respectively. Substitution of Eq. (4) into Eq. (2) and then into Eq. (1) gives the generalized diffusion equation, which is suitable for the averaged description of impurity transport under the condition that the concentration spatial scale is larger than the correlation length L, $L|\nabla c| \ll c$. The corresponding transport processes have a superdiffusion character, for which the migration distance varies as $r(t) \sim L(Vt/L)^{1/(2-\alpha)}$. An alternative formulation of this problem consists in using the formalism of fractional derivatives. The corresponding transport equation differs from the classical equation by the replacement of the second-order spatial derivatives by the derivatives of the order $2 - \alpha$. It should be emphasized that both formulations deal with the averaged description of the processes on the $|\mathbf{r}| \gg L$ scale.

Let us now consider the problem in which the size R of an impurity source can be on the order of or smaller than the correlation length L. Assume that the time intervals measured from the beginning of source action satisfy the inequality $t \gg L/V$. Let us surround the source with an imaginary surface S_1 with a characteristic radius $R_1 \gg L$. The surface shape is chosen so that the impurity concentration at the surface is constant for a point source placed at the origin coinciding with the center of the real source. The total impurity flux Q from the source to the surface can be represented as

$$Q = A(c_0 - c_1). \tag{5}$$

Here, c_0 and c_1 are the concentrations at the source surface S and the surface S_1, respectively, and the quantity A is determined by the properties of the medium between these surfaces (near zone). The flux Q is continuous at the surface S_1 and, hence, can be expressed in terms of the medium characteristics outside the surface S_1 (far zone), where the generalized transport equation holds:

$$Q = Bc_1. \tag{6}$$

By eliminating the concentration c_1 from Eqs. (5) and (6), one arrives at the relations

$$Q = KQ_0, \quad Q_0 = Bc_0, \quad K = A(A+B)^{-1}. \tag{7}$$

For a given concentration at the source surface, the quantity Q_0 corresponds to the source power in the absence of fluctuations of medium properties; Q is the effective power depressed due to fluctuations; and K is the power renormalization coefficient.

The coefficient B is calculated by the standard method using Eq. (1) and Eqs. (2) and (4). By the order of magnitude, it can be written as

$$B \sim VL^2(R_1/L)^{1+\alpha}. \tag{8}$$

At distances $|\mathbf{r}| \gg L$, the average concentration can be expressed in terms of the effective power Q, regardless of the source size. In particular, one can use Eq. (1) and Eqs. (2) and (4) to obtain the following expression for the far tail of concentration distribution in the case where the permanent source acts from $t = 0$:

$$c(\mathbf{r}, t) \propto Q\frac{t^2}{2}\frac{\partial f_i}{\partial x_i} \propto Q\frac{t^2}{|\mathbf{r}|^{5-\alpha}}. \tag{9}$$

Coefficient A cannot be derived from the generalized transport equation, because it requires knowledge of the distribution of medium characteristics in the near zone, where they strongly fluctuate. This situation resembles the problem of tunneling barrier conductivity explored by Raikh and Ruzin in [3]. Thus, we will use their approach. Like the conductivity in [3], the transmission coefficient A in our problem is determined by rare combinations of favorable conditions (e.g., cracks for the impurity transport in rocks), i.e., so-called "punctures." The contribution F to the transmission coefficient from an individual puncture is statistically distributed over a wide range of its values. This contribution can be expressed as $F = F_0\exp(-u)$, where u is the auxiliary variable taking values from 0 to ∞. As in [3], the puncture concentration per unit area of the source surface S can be determined by the expression

$$\rho(u) = (S_0)^{-1}\exp[-\Omega(u)]. \tag{10}$$

Here, $S_0^{1/2}$ is the characteristic cross-sectional size of the puncture, which is small compared to the average distance between the punctures, and $\Omega(u)$ is the function with the properties $\Omega(u) \gg 1$, $\partial\Omega/\partial u < 0$, $\partial^2\Omega/\partial u^2 > 0$. The ensemble-averaged transmission coefficient is

$$\langle A \rangle = S\frac{F_0}{S_0}\int_0^\infty du\, e^{-u - \Omega(u)}. \tag{11}$$

The integrand in this expression has a sharp peak. Because of this, one obtains from Eq. (11) with an accuracy of a pre-exponential factor

$$\langle A \rangle = Sa, \quad a \approx \frac{F_0}{S_0}\exp[-u_{\rm opt} - \Omega_{\rm opt}]. \tag{12}$$

Here, a is the specific transmission coefficient (independent of the source surface area), $\Omega_{\rm opt} = \Omega(u_{\rm opt})$, and the value $u = u_{\rm opt}$ corresponding to the optimal pinholes is determined from the relation $(\partial\Omega(u)/\partial u)_{u=u_{\rm opt}} + 1 = 0$. The condition for applicability of result (12) amounts to the requirement that the mean number of optimal punctures be large at the source surface, $S\rho(u_{\rm opt}) \gg 1$, or

$$S > S_*, \quad S_* = S_0\exp(\Omega_{\rm opt}). \tag{13}$$

For a small area of the surface S, $S < S_*$, and for the mean number of optimal punctures less than unity, the average transmission coefficient is determined by the integral in Eq. (11), in which the lower limit should be replaced by the value $u = u_f$ corresponding to the pinholes whose mean number for this area is on the order of unity, $S\rho(u_f) = 1$. Then, with an accuracy of the pre-exponential factor, one has

$$\langle A \rangle = S_* a\exp[-(u_f - u_{\rm opt})], \quad S < S_*. \tag{14}$$

By definition and according to Eqs. (10) and (13), the quantity u_f satisfies the equation

$$\frac{S}{S_*}\exp[\Omega_{\rm opt} - \Omega(u_f)] = 1. \tag{15}$$

Note that, whereas for large source sizes ($S > S_*$) the value $\langle A \rangle$ decreases proportionally to the area, it decreases, according to Eqs. (14) and (15), much faster for small sizes ($S < S_*$). One more effect caused by the fluctuations of the properties of a disordered medium consists of the increase in the statistical scatter of the transmission coefficient A with decreasing source size. The calculations analogous to those performed for the tunneling barrier conductivity in [3] suggest that the relative scatter $\Delta(A) = \langle(A - \langle A \rangle)^2\rangle^{1/2}/\langle A \rangle$ is small if $S > S_*$, comparable with unity if $S < S_*$, and may be larger than unity if $S \ll S_*$.

Taking into account the results obtained for the transmission coefficient and based on the estimate (8) and Eqs. (7), one can conclude that the power renormal-

ization coefficient tends to unity for large-sized sources ($K \cong 1$ if $S \gg S_*$) and that its mean value for small sizes ($S < S_*$) is determined by the expression

$$\langle K \rangle \cong \langle A \rangle / B \ll 1 \quad \text{at} \quad S \ll S_*. \tag{16}$$

As for A, the statistical scatter $\Delta(K)$ of the renormalization coefficient increases with a decrease in area. Naturally, the characteristic area S_* separating the domains of two different impurity transport regimes (the fluctuations are immaterial at $S > S_*$ and should be taken into account at $S < S_*$) is on the order of L^2.

Thus, the spatial fluctuations of medium characteristics suppress significantly the ensemble-averaged effective power for small-sized impurity sources.

In this case, the effective power also exhibits a large statistical scatter.

REFERENCES

1. J.-P. Bouchaund and A. Georges, Phys. Rep. **195**, 127 (1990).

2. K. V. Chukbar, Zh. Éksp. Teor. Fiz. **108**, 1875 (1995) [JETP **81**, 1025 (1995)].

3. M. E. Raikh and I. M. Ruzin, in *Mesoscopic Phenomena in Solids*, Ed. by B. L. Altshuler, P. A. Lee, and R. A. Webb (North-Holland, Amsterdam, 1991).

Translated by V. Sakun

On the Zel'dovich Regularization Method in the Theory of Quasistationary States

V. D. Mur[1], S. G. Pozdnyakov[1], V. S. Popov[2], and S. V. Popruzhenko[1]

[1] *Moscow Engineering Physics Institute (Technical University), Kashirskoe sh. 31, Moscow, 115409 Russia*
[2] *Institute for Theoretical and Experimental Physics, ul. Bol'shaya Cheremushkinskaya 25, Moscow, 117218 Russia*
Received February 7, 2002

Complex quasienergy and level width are calculated for a weakly bound atomic state in an intense circularly polarized monochromatic laser field using the method suggested by Zel'dovich for the regularization of divergent integrals with the Gamow wave function. It is demonstrated that this method converges, and the conditions for its applicability are indicated. These results are used to discuss the accuracy of the semiclassical approximation in the problems of ionization theory. © *2002 MAIK "Nauka/Interperiodica"*.

PACS numbers: 32.80.Rm; 31.15.Gy; 03.65.Sq

Quasistationary states whose Gamow wave functions increase exponentially at infinity, $|\chi_k(r)| \sim \exp(k_2 r)$, where $k = \sqrt{2E} = k_1 - ik_2$ is the momentum with $k_2 > 0$, frequently occur in the theory of elementary particles and atomic and nuclear physics. As a result, obvious difficulties arise when using a quantum mechanical apparatus, because even the normalization integral $\int_0^\infty |\chi_k(r)|^2 dr$ diverges. The method for overcoming this difficulty was pointed out by Zel'dovich in [1], where he suggested that the normalization integral should be understood in the regularized sense as the limit

$$N = \lim_{\alpha \to +0} \int_0^\infty \chi_k^2(r) \exp(-\alpha r^2) dr, \qquad (1)$$

which, in particular, allows one to construct perturbation theory for the quasistationary states [1, 2].

However, as far as we know, the Zel'dovich regularization method has not been applied to particular physical problems of quantum mechanics so far. In this work, we discuss the applicability of this method by the example of decay of an atomic level bound by the short-range forces in the field of a circularly polarized electromagnetic wave and indicate conditions for the applicability of this method.[1]

In the frame of reference rotating with the field [5], the Schrödinger equation becomes stationary with the Hamiltonian

$$H_\omega = -\frac{1}{2}\Delta + U(r) - \omega L_z + \mathcal{E}x, \qquad (2)$$

where $\hbar = m = e = 1$, ω and $\mathcal{E}$ are the frequency and the amplitude of the electric field, respectively, and L_z is the projection of the orbital angular momentum of an electron onto the direction of wave propagation. The spectrum of complex quasienergy levels coincides with the spectrum of quasistationary levels of the Hamiltonian H_ω.

We restrict ourselves to the *s* states and, as in [6, 7], use for $U(r)$ the zero-range approximation (δ potential). In the three-dimensional case, this is equivalent to the boundary condition [2]

$$\lim_{r \to 0} \frac{d}{dr}(r\psi)/(r\psi) = -\kappa_0, \qquad (3)$$

where $E_0 = -\kappa_0^2/2$ is the energy level in the absence of the wave. Taking into account the explicit analytical expression for the Green's function of (2) satisfying the Sommerfeld radiation condition at infinity, one arrives at the closed equation for the quasienergy $E = E_r - i\Gamma/2$ of the quasistationary state. This equation was obtained by Berson [6] and Manakov and Rapoport [7] and can be written as[2]

$$I(\epsilon; \gamma, K_0) = \sqrt{\epsilon} - 1, \qquad (4)$$

$$I = \frac{1}{(2\pi i K_0)^{1/2}} \int_0^\infty \frac{du}{u^{3/2}} \left\{ \exp\left(i\frac{2K_0}{\gamma^2}\frac{\sin^2 u}{u}\right) - 1 \right\} \times \exp(-2iK_0\epsilon u). \qquad (4a)$$

---

[1] This problem is also of interest in the theory of multiphoton ionization of the negative ions of the type H⁻, Li⁻, Na⁻, etc. Numerous results achieved in this area are discussed in monograph [3] and review [4].

[2] See also [3, 4]. Equation (4) was generalized in [8] to the states with nonzero orbital angular momentum l, with allowance for the effective radius of interaction (this is substantial for $l \geq 1$, because the zero-range approximation does not apply if $l \neq 0$).
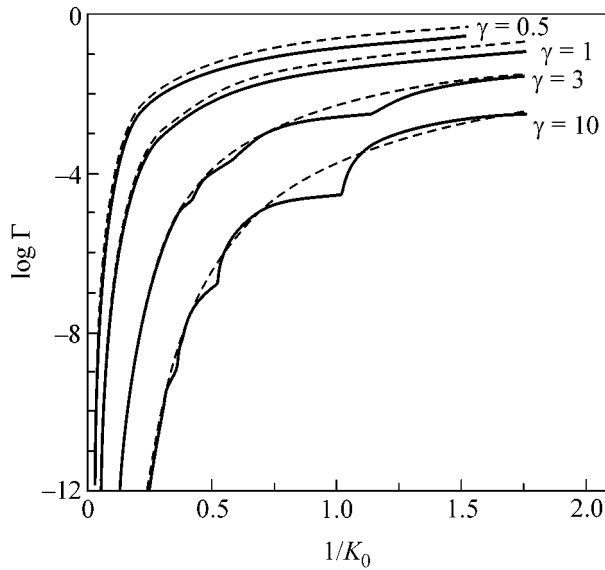
Fig. 1. Level width Γ vs. $1/K_0 = 2\omega$. The solid lines are the numerical calculations by Eq. (6), and the dashed lines are the semiclassical approximation Γ_Q. Each curve is labeled Keldysh parameter γ; the ordinate-axis scale is logarithmic.
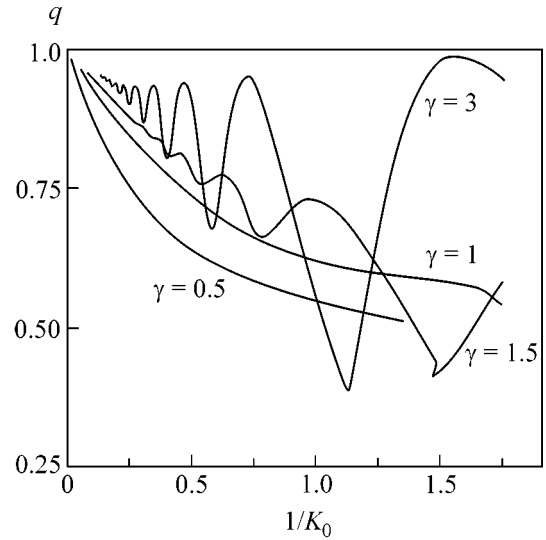

Fig. 2. Accuracy of quasiclassical approximation: the ratio $q = \Gamma/\Gamma_Q$ against $1/K_0$.

Here,

$$\epsilon = \varepsilon + \gamma^{-2}, \quad \varepsilon = E/E_0 = 1 + \delta + i\kappa_0^{-2}\Gamma, \tag{5}$$
$$\delta = (E_r - E_0)/E_0,$$

$$\gamma = \omega\kappa_0/\mathscr{E} = 1/2K_0F, \quad K_0 = |E_0|/\omega, \tag{5a}$$
$$F = \mathscr{E}/\kappa_0^3,$$

where ε and F are the reduced quasienergy and the electric field, respectively, γ is the Keldysh adiabaticity parameter [9], and K_0 is the multiquantum parameter of the process. Taking into account that the scaling relationships $\Gamma \propto \kappa_0^2$ and $\mathscr{E} \propto \kappa_0^3$ are fulfilled in the δ-potential model, we set $\kappa_0 = 1$ without loss of generality.

Since $\mathrm{Im}\,\epsilon = \Gamma > 0$ for the quasistationary state, integral (4a) diverges exponentially at the upper limit and requires regularization. In this case, the regularization reduces to the analytic continuation of Eq. (4a) from the lower ϵ half-plane, where the integral is well defined. For this purpose, we use the Zel'dovich method, i.e., assume that the $\alpha \longrightarrow +0$ limit of the solutions to the equation

$$I_\alpha(\epsilon; \gamma, K_0) = \sqrt{\epsilon} - 1 \tag{6}$$

is the solution to Eq. (4); I_α differs from I only by the factor $\exp(-\alpha u^2)$ in the integrand. To illustrate that the Zel'dovich method converges, we consider a characteristic example. The numerical solution to Eq. (6) gives the following for $\gamma = 3$ and $K_0 = 1.5$: $\delta = 3.89207(-3)$ and $\Gamma = 6.27485(-4)$, $\delta = 3.89202(-3)$ and $\Gamma = 6.27398(-4)$,

and $\delta = 3.892006(-3)$ and $\Gamma = 6.27370(-4)$ for $\sqrt{\alpha} = 2.0(-3)$, $1.0(-3)$, and $2.5(-4)$, respectively, while the extrapolation to the $\alpha = 0$ yields $\delta = 3.892005(-3)$ and $\Gamma = 6.27369(-4)$. Here, $a(b) \equiv a \times 10^b$. To calculate Γ with the relative accuracy 10^{-5}, it is usually necessary to achieve the values $\alpha \leq 10^{-4}$–10^{-5}, with the convergence of the method being 1–2 orders of magnitude higher for the Stark shift δ than for Γ.

The results of calculation of the widths Γ for different values of the Keldysh parameter are shown in Fig. 1. It is seen that the behavior of Γ in the antiadiabatic region $\gamma > 1$ exhibits irregularities caused by opening or closing the successive channel of n-photon ionization. At the same time, the level width for $\gamma \leq 1$ depends monotonically on the field frequency. Figure 1 also shows the semiclassical Γ_Q values calculated by the formulas obtained in [10, 11]. The accuracy of the semiclassical approximation can be judged in more detail from Fig. 2, where the ratio $q(\gamma, K_0) = \Gamma/\Gamma_Q$ is shown. At $\gamma < 1$, this ratio decreases monotonically with multiquantum parameter K_0, while it exhibits oscillations due to the threshold effects as γ increases. In the limit $K_0 \longrightarrow +\infty$, the semiclassical approximation becomes exact for any γ. Finally, Fig. 3 shows the width Γ as a function of the field F for several values of $\omega = 1/2K_0$. The function $\Gamma(F, \omega)$ shows characteristic discontinuities in the vicinity of the n-photon ionization thresholds ($K_0 = n$ at $\gamma \gg 1$). The calculation of the width encounters difficulties in these regions of parameters, because Eq. (6) has no limit there. Thus, the Zel'dovich method does not apply in narrow regions near the ionization threshold.

To reveal the cause for this fact, let us consider the integral

$$J(\varepsilon, s) = \int_0^\infty dt\, t^{s-1} \exp\{-i\varepsilon t\} = \Gamma(s)(i\varepsilon)^{-s}, \quad (7)$$

$$\varepsilon = \varepsilon_1 + i\varepsilon_2,$$

which converges in the lower ε half-plane. Introducing Zel'dovich regularization, one obtains

$$J_\alpha(\varepsilon, s) = \int_0^\infty dt\, t^{s-1} \exp\{-i\varepsilon t - \alpha t^2\} \quad (8)$$

$$= \Gamma(s)(2\alpha)^{-s/2} \exp(-\varepsilon^2/8\alpha) \mathcal{D}_{-s}(i\varepsilon/2\alpha),$$

where $\mathcal{D}_{-s}(z)$ is the parabolic cylinder function. At $\alpha \longrightarrow 0$, this gives

$$J_\alpha(\varepsilon, s) = \Gamma(s)(i\varepsilon)^{-s}\{1 + O(\exp(-\varepsilon^2/8\alpha))\}, \quad (9)$$

where the correction in the braces is written with the pre-exponential accuracy. If $\varepsilon_1^2 - \varepsilon_2^2 > 0$, this formula reduces to Eq. (7) in the limit $\alpha \longrightarrow +0$. However, at $\varepsilon_1^2 - \varepsilon_2^2 < 0$, the second term in Eq. (9) increases exponentially and J_α has no limit, which is caused by the Stokes phenomenon known in the theory of asymptotic expansions.

Thus, the Zel'dovich recipe (1) applies to the quasistationary state with momentum $k = k_1 - ik_2$ if

$$|k_1| > k_2, \quad (10)$$

i.e., if the width of the level is smaller than its distance from the threshold. This condition (not pointed out in [1, 2]) is usually satisfied (and even with a margin). However, when considering the dynamic Stark effect in a strong field [particularly, when solving Eq. (6)], inequality (10) may be broken and the Zel'dovich method becomes inapplicable, as is manifested by the presence of discontinuities in the curves in Fig. 3.

The question then arises of whether it would be more profitable to use in Eq. (6) the regulators decreasing even more rapidly at infinity, e.g., as $\exp(-\alpha u^4)$. It turned out that such is not the case. Numerical analysis of this case shows that the convergence at $\alpha \longrightarrow +0$ becomes even worse and the region of applicability of the method becomes narrower: $|k_2| < 0.41|k_1|$ instead of Eq. (10). One can show that for the regulator of the form $R_\lambda = \exp(-\alpha u^\lambda)$ the method converges within the angle

$$k_2 < |k_1| \tan\frac{\pi}{2\lambda}, \quad \lambda > 1. \quad (11)$$

At $\lambda \longrightarrow \infty$, i.e., for $R_\infty = \exp(-\alpha e^u)$, the regularization fails for any $k_2 > 0$. In this sense, the Zel'dovich regularization method is optimal.
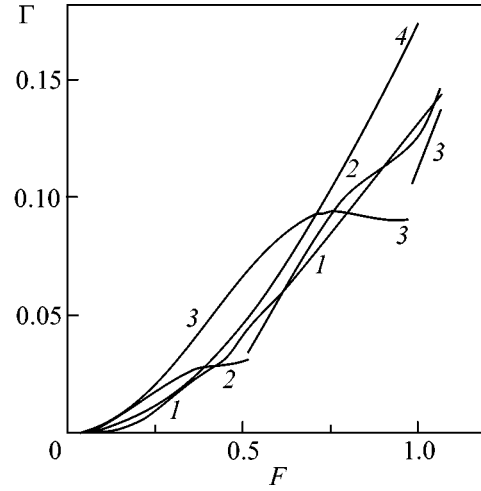
Fig. 3. Width Γ vs. the reduced electric field F for $\omega =$ (*1*) 0.5, (*2*) 0.75, (*3*) 1.0, and (*4*) 1.5.

Note that a similar situation takes place in the theory of divergent series [12]: although there are very powerful methods for summing some rapidly divergent series, these methods become inoperative in the case of a slightly divergent series such as $1 - 1 + 1 - 1 + \ldots = 1/2$.

In conclusion, we note that previous calculations [3, 7] of the width Γ as a function of the parameters γ and ω in the δ-potential model are in sharp contradiction with Fig. 1 and, in our opinion, are incorrect (as was already pointed out in [8]). Recently, Manakov *et al.* [13] suggested for Eq. (4) the regularization method, which considerably differs from the Zel'dovich method.[3] The Γ values obtained by this method agree with our results (cf. curve *2* in Fig. 3 with the corresponding curve in Fig. 1 from [14]). However, the Zel'dovich regularization method is far more universal and, in our opinion, will find further use in the theory of quasistationary states.

REFERENCES

1. Ya. B. Zel'dovich, Zh. Éksp. Teor. Fiz. **39**, 776 (1961) [Sov. Phys. JETP **12**, 542 (1961)].

2. A. I. Baz', Ya. B. Zel'dovich, and A. M. Perelomov, *Scattering, Reactions, and Decays in Nonrelativistic Quantum Mechanics* (Nauka, Moscow, 1971, 2nd ed.; Israel Program for Scientific Translations, Jerusalem, 1966), Chap. 7.

[3] This method was used in [13, 14] to consider the process of stabilization in a strong field, and the rate of ionization of a negative hydrogen ion by laser radiation was calculated.

3. L. P. Rapoport, B. A. Zon, and N. L. Manakov, *Theory of Multiphoton Processes in Atoms* (Atomizdat, Moscow, 1978).

4. N. L. Manakov, M. L. Frolov, A. F. Starace, and I. I. Fabricant, J. Phys. B **33**, R141 (2000).

5. F. V. Bunkin and A. M. Prokhorov, Zh. Éksp. Teor. Fiz. **46**, 1090 (1964) [Sov. Phys. JETP **19**, 739 (1964)].

6. I. J. Berson, J. Phys. B **8**, 3078 (1975).

7. N. L. Manakov and L. P. Rapoport, Zh. Éksp. Teor. Fiz. **69**, 842 (1975) [Sov. Phys. JETP **42**, 430 (1975)].

8. S. P. Andreev, B. M. Karnakov, V. D. Mur, and V. A. Polunin, Zh. Éksp. Teor. Fiz. **86**, 866 (1984) [Sov. Phys. JETP **59**, 506 (1984)].

9. L. V. Keldysh, Zh. Éksp. Teor. Fiz. **47**, 1945 (1964) [Sov. Phys. JETP **20**, 1307 (1964)].

10. A. I. Nikishov and V. I. Ritus, Zh. Éksp. Teor. Fiz. **50**, 255 (1966) [Sov. Phys. JETP **23**, 168 (1966)].

11. A. M. Perelomov, V. S. Popov, and M. V. Terent'ev, Zh. Éksp. Teor. Fiz. **51**, 309 (1966) [Sov. Phys. JETP **24**, 207 (1967)].

12. G. H. Hardy, *Divergent Series* (Clarendon, Oxford, 1949; Inostrannaya Literatura, Moscow, 1951).

13. N. L. Manakov, M. V. Frolov, B. Borca, and A. F. Starace, Pis'ma Zh. Éksp. Teor. Fiz. **72**, 426 (2000) [JETP Lett. **72**, 294 (2000)].

14. M. V. Frolov, N. L. Manakov, B. Borca, and A. F. Starace, J. Phys. B **34**, L579 (2001).

Translated by R. Tyapaev